

Heterogeneous & Homogeneous & Bio- & Nano-

CHEM **CAT** CHEM

CATALYSIS

Accepted Article

Title: Design of ordered mesoporous sulfonic acid functionalized ZrO₂/organosilica bifunctional catalysts for direct catalytic conversion of glucose to ethyl levulinate

Authors: Daiyu Song, Qingqing Zhang, Yingnan Sun, Panpan Zhang, Yi-Hang Guo, and Jianglei Hu

This manuscript has been accepted after peer review and appears as an Accepted Article online prior to editing, proofing, and formal publication of the final Version of Record (VoR). This work is currently citable by using the Digital Object Identifier (DOI) given below. The VoR will be published online in Early View as soon as possible and may be different to this Accepted Article as a result of editing. Readers should obtain the VoR from the journal website shown below when it is published to ensure accuracy of information. The authors are responsible for the content of this Accepted Article.

To be cited as: *ChemCatChem* 10.1002/cctc.201801089

Link to VoR: <http://dx.doi.org/10.1002/cctc.201801089>

Design of ordered mesoporous sulfonic acid functionalized ZrO₂/organosilica bifunctional catalysts for direct catalytic conversion of glucose to ethyl levulinate

Daiyu Song,^[a] Qingqing Zhang,^[a] Yingnan Sun,^[a] Panpan Zhang,^[a] Yi-Hang Guo,^{*[a]} and Jiang-Lei Hu^{*[b]}

Dedication ((optional))

Abstract: Ordered mesoporous sulfonic acid functionalized ZrO₂/organosilica catalysts (SO₄²⁻/ZrO₂-PMO-SO₃H) bearing tunable Brønsted and Lewis acid site distributions were prepared by a P123-directed sol-gel co-condensation route followed by ClSO₃H functionalization. As-prepared catalysts were applied in the conversion of glucose to ethyl levulinate in ethanol medium. The SO₄²⁻/ZrO₂-PMO-SO₃H-catalyzed target reaction followed a glucose–ethyl glucoside–ethyl fructoside–5-ethoxymethylfurfural–ethyl levulinate pathway dominated by the synergistic effect of the super strong Brønsted acidity and moderate Lewis acidity of the catalysts. Additionally, by combining the advantages of the considerably high Brønsted (696 μeq g⁻¹) and Lewis acid site density (703 μeq g⁻¹), optimal Brønsted/Lewis molar ratio (0.99) and excellent porosity properties, the SO₄²⁻/ZrO₂-PMO-SO₃H1.0 obtained at an initial Si/Zr molar ratio of 1.0 exhibited the highest ethyl levulinate yield (42.3%) among the various tested catalysts. Moreover, the SO₄²⁻/ZrO₂-PMO-SO₃H can be reused three times without obvious changes in activity, morphology and chemical structure.

Introduction

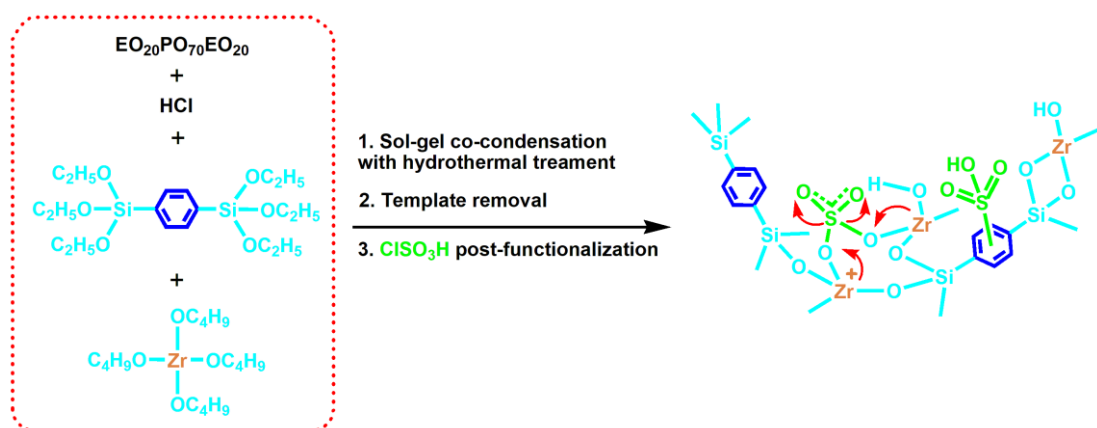
Catalytic conversion of lignocellulosic biomass/derivatives to alternative and renewable biofuels is currently of great interest to alleviate the dependency on rapidly decreasing fossil reserves and to reduce the emissions of greenhouse and noxious gases such as CO, CO₂, NO_x and SO_x.^[1] The 'first generation' biofuels are typically represented by biodiesels, which are composed of a mixture of C₁₂–C₂₂ fatty acid methyl esters derived from acid/base-catalyzed transesterification of oily feedstocks with light alcohols.^[2,3] Owing to enormous market requirements, the 'second generation' biofuels, which are obtainable directly via

chemical or biochemical transformation of lignocellulosic biomass/derivatives, has emerged more recently. Bio-ethanol, biomass-derived furanic compounds as well as alkyl levulinates represent a large family of the 'second generation' biofuels that can be blended directly with fossil fuels.^[4] Among them, alkyl levulinates have been proposed as promising candidates.^[5,6] Among the various alkyl levulinates, including methyl, ethyl and butyl levulinate, ethyl levulinate (EL) is the most suitable fuel blend in terms of miscibility, reduced emissions and shorter degradation time. EL can be directly used in diesel engines.^[6,7] EL can be synthesized by acid-catalyzed ethanolysis of various biomass-derived substrates such as levulinic acid (LA), furfuryl alcohol (FAL), monosaccharides, disaccharides and polysaccharides.^[7] Although high EL yield is obtained from LA or FAL, the higher price of LA or FAL due to the multistep biomass transformation process used for their production leads to an uneconomical EL production process. For acid-catalyzed direct conversion of disaccharides or polysaccharides to EL without separating intermediates such as LA, 5-hydroxymethylfurfural (5-HMF) or 5-ethoxymethylfurfural (5-EMF) and byproducts from the reaction mixture, the yield of EL is considerably low (lower than 50%) due to poor selectivity for EL.^[8,9] Acid-catalyzed direct synthesis of EL from monosaccharides such as fructose or glucose in ethanol medium has been the most favorable approach, and fructose is reported to give a significantly higher EL yield compared to glucose.^[10-12] Sustainable glucose is more cheap and abundant than fructose; however, direct conversion of glucose to EL is more complex and difficult than conversion of fructose because the process involves isomerization of glucose/ethyl glucoside to fructose/ethyl fructoside catalyzed predominantly by Lewis (L) acid sites.^[13-17] Subsequent successive dehydration of fructose/or ethyl fructoside to EL is mainly catalyzed by Brønsted (B) acid sites. From an ecological and economical viewpoint, bifunctional catalyst systems bearing both B and L acid sites for the direct production of EL from abundant biomass-derived glucose can provide a highly desirable alternative approach that obviates the dependence on LA or FAL.^[9] For this purpose, SO₄²⁻/ZrO₂, protonic forms of aluminosilicate zeolites such as Hβ, HUSY, HZSM-5, HMOR and HY have been applied in such conversion process.^[9] However, the catalytic activity and selectivity of the aforementioned systems are unsatisfactory because of moderate B and/or L acidity or inferior porosity properties. Therefore, the design of robust, efficient and recyclable bifunctional solid acid catalysts for glucose conversion to alkyl levulinates remains a challenge.

[a] Dr. D. Song, Dr. Q. Zhang, Dr. Y. Sun, Dr. P. Zhang, Prof. Y.-H. Guo*
School of Environment
Northeast Normal University
Changchun 130117, P.R. China
Tel./Fax: (+86)431-89165626
E-mail: guoyh@nenu.edu.cn

[b] Dr. J.-L. Hu*
School of Chemical Engineering
Changchun University of Technology
Changchun 130012, P.R. China

Supporting information for this article is given via a link at the end of the document. ((Please delete this text if not appropriate))



Scheme 1. Illustrations of the preparation route and wall structure of bifunctional $\text{SO}_4^{2-}/\text{ZrO}_2\text{-PMO-SO}_3\text{H}$ catalysts.

Recently reported combined catalyst systems consisting of $\text{SO}_4^{2-}/\text{ZrO}_2$ (strong B acidity and moderate L acidity) and Sn-Beta zeolites (considerably high L acidity) have been found to exhibit superior catalytic activity compared to conventional acid catalysts in the direct conversion of glucose in methanol to methyl levulinate.^[9]

Motivated by the above considerations, here, a series of highly ordered mesoporous sulfonic acid functionalized ZrO_2 /organosilica catalysts with strong B acidity and moderate L acidity as well as tunable acid site distributions were prepared by a carefully designed P123-directed sol-gel co-condensation route followed by ClSO_3H functionalization. The resulting bifunctional $\text{SO}_4^{2-}/\text{ZrO}_2\text{-PMO-SO}_3\text{H}$ catalysts with superior porosity properties, including a large BET surface area, high pore volume and surface hydrophobicity, were successfully applied in the conversion of glucose to EL in ethanol medium. Special attention was paid to studying the reaction pathway and kinetics of the $\text{SO}_4^{2-}/\text{ZrO}_2\text{-PMO-SO}_3\text{H}$ -catalyzed glucose conversion on the basis of qualitative and quantitative analyses of the product distribution, to reveal the contributions of the B and L acid sites of the catalysts to the formation of EL.

Results and Discussion

Preparation and characterization of bifunctional $\text{SO}_4^{2-}/\text{ZrO}_2\text{-PMO-SO}_3\text{H}$ catalysts

As illustrated in Scheme 1, ordered mesoporous bifunctional $\text{SO}_4^{2-}/\text{ZrO}_2\text{-PMO-SO}_3\text{H}$ catalysts were facilely prepared by a P123-directed co-hydrolysis and -condensation of the bridging organosilane BTESB and $\text{Zr}(\text{OnBu})_4$ under acidic condition followed by ClSO_3H functionalization. In the first step, the key factor for ensuring a $\text{ZrO}_2\text{-PMO}$ framework with highly ordered mesostructure is to optimize the molar composition of the starting materials, which affects the hydrolysis and condensation rates of BTESB and $\text{Zr}(\text{OnBu})_4$ as well as the hydrophilicity/hydrophobicity of the preparation system.

Accordingly, the morphologies of lyotropic liquid crystal phases were well-adjusted. Here, the molar composition was controlled at P123: BTESB: $\text{Zr}(\text{OnBu})_4$: HCl : H_2O = 0.029: 1: (0.5, 1 or 2): 4.4: 288. At this molar composition, P123 micelles can aggregate linearly to form cylindrically shaped lyotropic liquid crystal structures, and the interaction between the cylindrical P123 liquid crystals and the hydrolyzed Si/Zr precursors ensured the construction of a $-\text{Zr}-\text{O}-\text{Si}-\text{C}_6\text{H}_4-\text{Si}-$ framework with ordered mesostructure. Additionally, the hydrolysis rate of BTESB was slower than that of $\text{Zr}(\text{OnBu})_4$. To ensure a matched hydrolysis rate of both precursors for adequate fabrication of the $-\text{Zr}-\text{O}-\text{Si}-\text{C}_6\text{H}_4-\text{Si}-$ framework, prehydrolysis of BTESB at 40 °C for 1 h was performed at the beginning of the catalyst preparation. The $-\text{Zr}-\text{O}-\text{Si}-\text{C}_6\text{H}_4-\text{Si}-$ framework was further fixed after hydrothermal treatment, and then $\text{ZrO}_2\text{-PMO}$ with a 2D hexagonal mesostructure was obtained after removal of P123. Subsequent functionalization of the $\text{ZrO}_2\text{-PMO}$ framework with ClSO_3H gave rise to bifunctional $\text{SO}_4^{2-}/\text{ZrO}_2\text{-PMO-SO}_3\text{H}$ catalysts without changing the structural ordering of the $\text{ZrO}_2\text{-PMO}$. However, at the lowest Si/Zr molar ratio of 0.25, $\text{SO}_4^{2-}/\text{ZrO}_2\text{-PMO-SO}_3\text{H}$ exhibited a disordered 3D interconnected mesostructure (see Figure 1b), implying that an unsuitable BTESB/ $\text{Zr}(\text{OnBu})_4$ ratio could not maintain the cylindrically shaped lyotropic liquid crystal structures. Additionally, the acid site distributions or molar ratio of B-to-L acid sites (n_B/n_L) can be adjusted by changing the initial Si/Zr molar ratio (Table 1).

Morphological characteristics

The TEM images presented in Figure 1a revealed that ZrO_2 -free $\text{PMO-SO}_3\text{H}$ exhibited a 2D hexagonal mesostructure with long-range structural ordering, and the estimated pore diameter was 6 nm. The $\text{SO}_4^{2-}/\text{ZrO}_2\text{-PMO-SO}_3\text{H}0.25$ catalyst obtained at an initial Si/Zr molar ratio of 0.25 exhibited a disordered 3D interconnected mesostructure with a pore diameter of ca. 4 nm (Figure 1b).

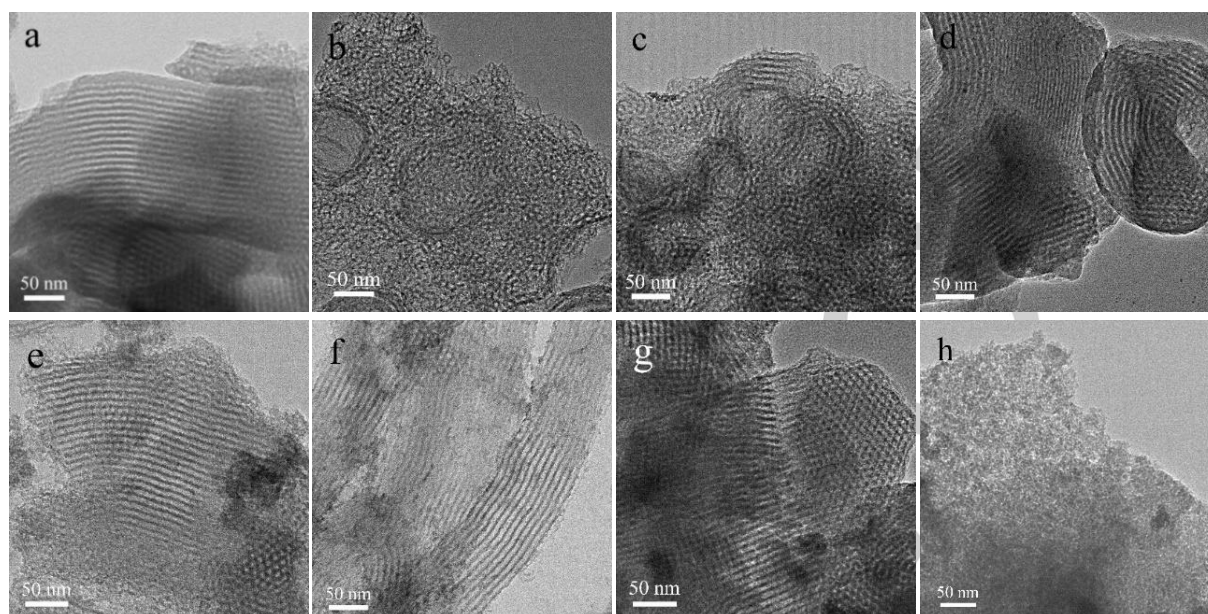


Figure 1. TEM images of PMO-SO₃H (a), SO₄²⁻/ZrO₂-PMO-SO₃H0.25 (b), SO₄²⁻/ZrO₂-PMO-SO₃H0.5 (c), SO₄²⁻/ZrO₂-PMO-SO₃H1.0 (d), SO₄²⁻/ZrO₂-PMO-SO₃H2.0 (e), SO₄²⁻/Nb₂O₅-PMO-SO₃H1.0 (f), SO₄²⁻/TiO₂-PMO-SO₃H1.0 (g) and PF-SO₄²⁻/ZrO₂-PMO-SO₃H1.0 (h).

Table 1 Textural parameters and acidic nature of various mesoporous sulfonated ZrO₂-organosilicas.

Catalyst	S_{BET}^a (m ² g ⁻¹)	D_p^b (nm)	V_p^c (cm ³ g ⁻¹)	A_B^d (μeq g ⁻¹)	A_L^e (μeq g ⁻¹)	n_B/n_L^f
PMO-SO ₃ H	1120	6.4	1.33	537	n.d.	n.d.
SO ₄ ²⁻ /ZrO ₂ -PMO-SO ₃ H2.0	959	6.4	1.31	566	572	0.99
SO ₄ ²⁻ /ZrO ₂ -PMO-SO ₃ H1.0	920	5.5	1.07	696	703	0.99
SO ₄ ²⁻ /ZrO ₂ -PMO-SO ₃ H0.5	900	3.9	0.68	986	835	1.18
SO ₄ ²⁻ /ZrO ₂ -PMO-SO ₃ H0.25	562	3.9	0.73	908	609	1.49
PF-SO ₄ ²⁻ /ZrO ₂ -PMO-SO ₃ H1.0	637	3.5	0.56	493	498	0.99
SO ₄ ²⁻ /Nb ₂ O ₅ -PMO-SO ₃ H1.0	793	5.6	1.09	682	710	0.96
SO ₄ ²⁻ /TiO ₂ -PMO-SO ₃ H1.0	700	6.4	1.00	595	661	0.90
SO ₄ ²⁻ /ZrO ₂ -SiO ₂ 1.0	314	4.2	0.72	545	458	1.19
HY zeolite	700	2.5	n.d.	647	n.d.	n.d.
Hβ zeolite	640	0.7	n.d.	423	n.d.	n.d.

^a The BET surface area (S_{BET}) was calculated using Brunauer–Emmett–Teller (BET) equation.

^b The pore diameter (D_p) was estimated from BJH adsorption determination.

^c The pore volume (V_p) was estimated from the pore volume determination using the adsorption branch of the N₂ isotherm curve at $P/P_0 = 0.99$ single point.

^d A_B : B acid site density.

^e A_L : L acid site density.

^f The molar ratio of B acid-to-L acid (n_B/n_L) was estimated by the peak area integral ratio at 1593 and 1443 cm⁻¹ (Figure 4c).

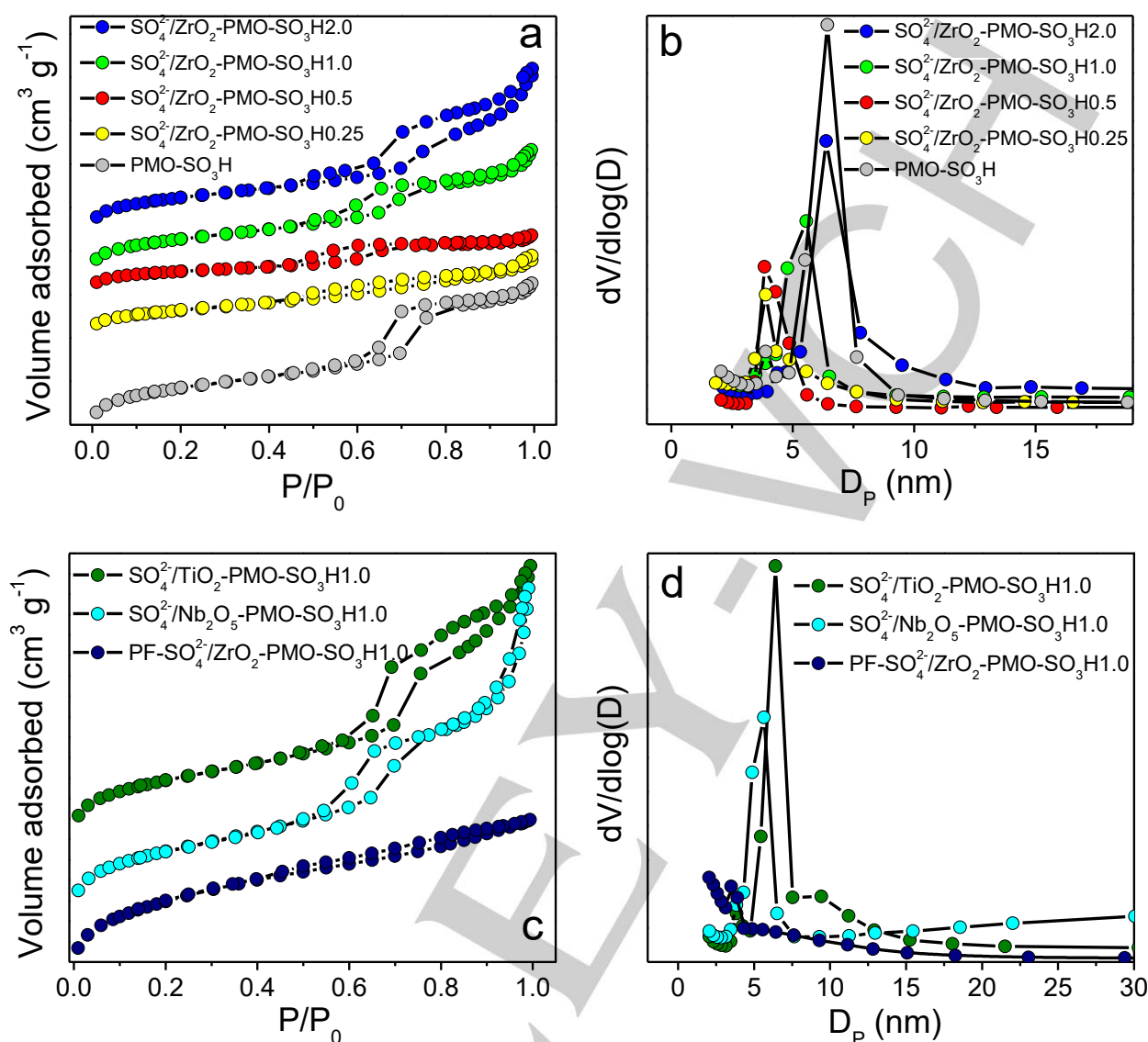


Figure 2. Nitrogen gas adsorption–desorption isotherms (a, c) and BJH pore size distribution profiles (b, d) of various SO₃H-based catalysts.

The SO₄²⁻/ZrO₂-PMO-SO₃H0.5, SO₄²⁻/ZrO₂-PMO-SO₃H1.0 and SO₄²⁻/ZrO₂-PMO-SO₃H2.0 catalysts obtained at initial Si/Zr molar ratios of 0.5, 1.0 and 2.0 all possessed an ordered mesostructure (pore diameter of 4–6 nm) with helically arranged mesopores (Figure 1c–e).

To verify the reproducibility of the aforementioned preparation route, SO₄²⁻/Nb₂O₅-PMO-SO₃H1.0 and SO₄²⁻/TiO₂-PMO-SO₃H1.0 were also prepared. As shown in Figure 1f and g, both samples exhibited ordered mesostructures similar to their SO₄²⁻/ZrO₂-PMO-SO₃H1.0 counterpart.

However, in the absence of P123, the resulting PF-SO₄²⁻/ZrO₂-PMO-SO₃H1.0 exhibited a 3D interconnected mesostructure (Figure 1h). The results suggested that P123 plays a structure-directing function in the formation of the SO₄²⁻

/ZrO₂(Nb₂O₅ or TiO₂)-PMO-SO₃H with an ordered mesostructure; in addition, the suitable molar composition of P123: BTESEB: Zr(O*n*Bu)₄: HCl: H₂O greatly influenced the structural ordering of the materials.

SAXS measurements supported the TEM observations. As shown in Figure S1 in the Supporting Information (SI), ZrO₂-free PMO-SO₃H exhibited three diffraction peaks in the low-angle range, *i.e.*, 0.7–1.1 deg (100), 1.5–1.7 deg (110) and 1.7–1.8 deg (200). The first peak possessed the highest intensity, whereas the other two peaks showed very weak intensity. The results indicated that the PMO-SO₃H possessed highly ordered mesoporous channels.

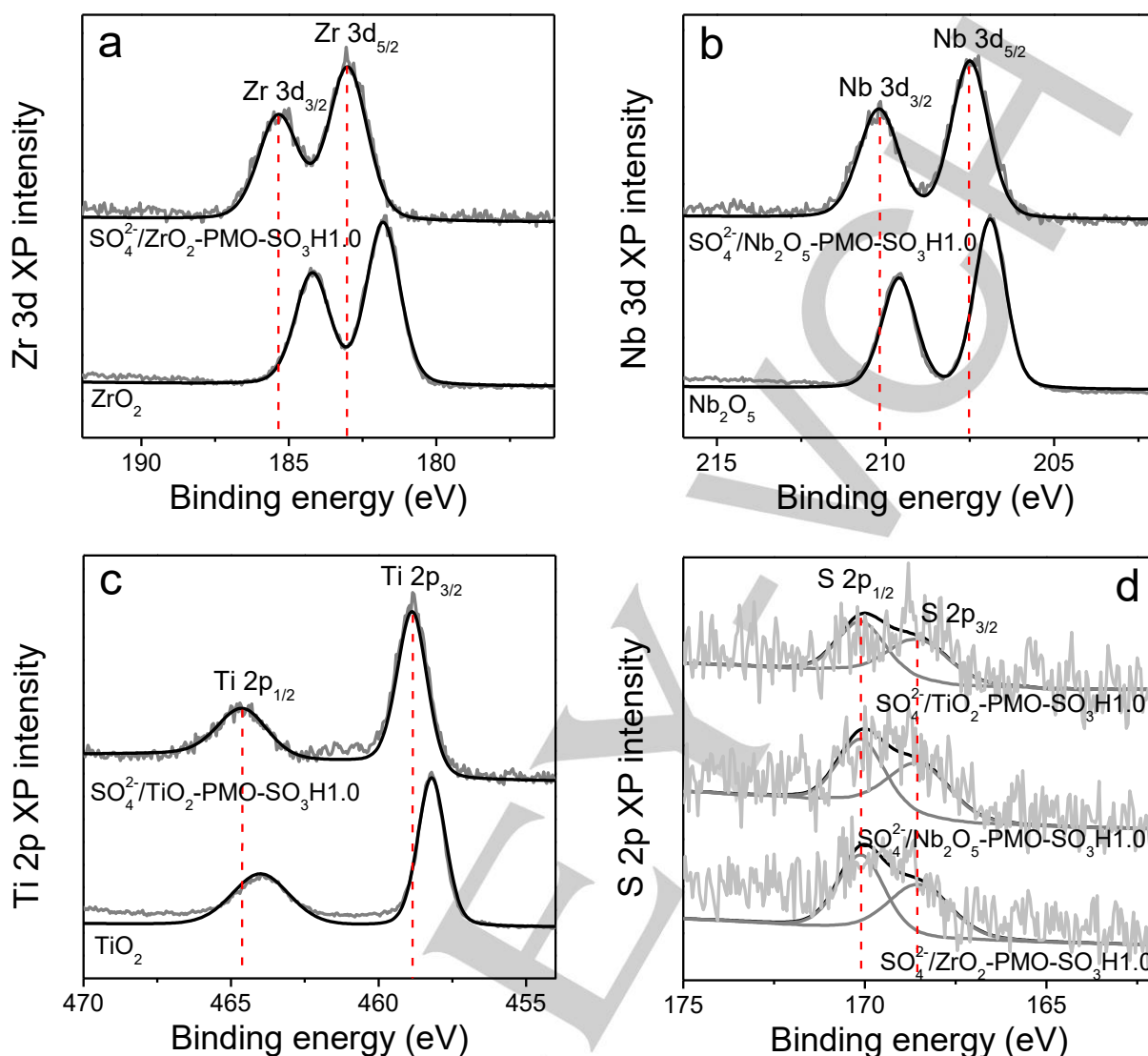


Figure 3. High resolution XPS spectra of SO₄²⁻/ZrO₂-PMO-SO₃H1.0 and ZrO₂ in the Zr 3d binding energy region (a), SO₄²⁻/Nb₂O₅-PMO-SO₃H1.0 and Nb₂O₅ in the Nb 3d binding energy region (b), SO₄²⁻/TiO₂-PMO-SO₃H1.0 and TiO₂ in the Ti 2p binding energy region (c) and SO₄²⁻/ZrO₂(Nb₂O₅/TiO₂)-PMO-SO₃H1.0 in the S 2p binding energy region (d).

For the sulfonated ZrO₂-PMO catalysts, the (100) diffraction peak (0.86–0.95 deg) gradually became weaker as the Si/Zr molar ratio decreased from 2.0, 1.0 to 0.5; in addition, the pair of weak diffraction peaks nearly disappeared. These results indicated that the SO₄²⁻/ZrO₂-PMO-SO₃H possessed structural ordering that decreased with increasing ZrO₂ content. In the case of PF-SO₄²⁻/ZrO₂-PMO-SO₃H1.0, the diffraction peaks in the low angle range were not found, further indicating its disordered mesostructure.

Therefore, bridging organosilica units (–Si–C₆H₄–Si–) and P123 with suitable content in the initial catalyst preparation system are important contributors to the structural ordering of the bifunctional catalysts.

Porosity properties

The porosity properties of the SO₄²⁻/ZrO₂-PMO-SO₃H catalysts were characterized by nitrogen porosimetry measurements. As shown in Figure 2a, PMO-SO₃H and SO₄²⁻/ZrO₂-PMO-SO₃H with Si/Zr molar ratios of 0.5, 1.0 and 2.0 exhibited a type IV isotherm with an H1 type hysteresis loop, reflecting their regular mesoporous structures without interconnecting channels. In addition, SO₄²⁻/ZrO₂-PMO-SO₃H0.25 had a type IV isotherm with an H2 type hysteresis loop, indicating its disordered mesostructure. These results are in consistent with those of obtained by TEM or SAXS.

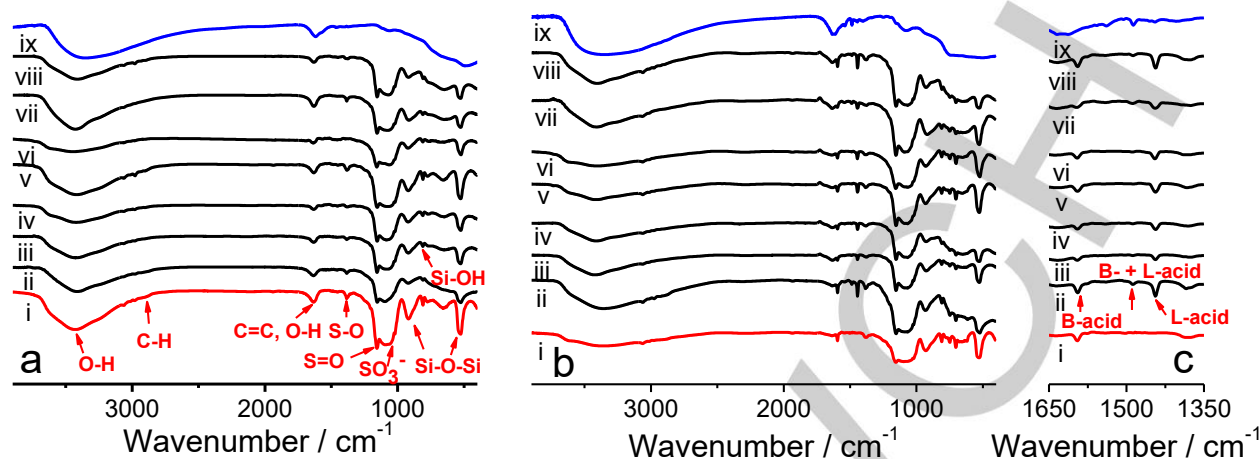


Figure 4. FTIR spectra (a) and pyridine-adsorbed FT-IR spectra (b, c) of (i) PMO-SO₃H, (ii) SO₄²⁻/ZrO₂-PMO-SO₃H0.25, (iii) SO₄²⁻/ZrO₂-PMO-SO₃H0.5, (iv) SO₄²⁻/ZrO₂-PMO-SO₃H1.0, (v) SO₄²⁻/ZrO₂-PMO-SO₃H2.0, (vi) PF-SO₄²⁻/ZrO₂-PMO-SO₃H1.0, (vii) SO₄²⁻/Nb₂O₅-PMO-SO₃H1.0, (viii) SO₄²⁻/TiO₂-PMO-SO₃H1.0 and (ix) ZrO₂.

Additionally, the aforementioned samples possessed narrowed BJH pore size distribution curves, indicating their well-distributed pore diameters (Figure 2b).

As shown in Figure 2c and d, both SO₄²⁻/Nb₂O₅-PMO-SO₃H1.0 and SO₄²⁻/TiO₂-PMO-SO₃H1.0 exhibited similar porosity properties to their SO₄²⁻/ZrO₂-PMO-SO₃H1.0 counterpart, indicating their ordered mesostructures with well-distributed pore size. However, the PF-SO₄²⁻/ZrO₂-PMO-SO₃H1.0 sample exhibited an ill-defined nitrogen gas sorption isotherm and pore size distribution curve, indicating a disordered mesostructure. The results further confirmed that the structural ordering of the bifunctional SO₄²⁻/ZrO₂(Nb₂O₅/TiO₂)-PMO-SO₃H catalysts was dominantly influenced by the Si/Zr molar ratio and structure-directing function of P123.

As summarized in Table 1, PMO-SO₃H exhibited the largest BET surface area (1120 m² g⁻¹) and the highest pore volume (1.33 m³ g⁻¹) among all tested samples. For three ordered mesoporous bifunctional catalysts, SO₄²⁻/ZrO₂-PMO-SO₃H2.0 (959 m² g⁻¹), SO₄²⁻/ZrO₂-PMO-SO₃H1.0 (920 m² g⁻¹) and SO₄²⁻/ZrO₂-PMO-SO₃H0.5 (900 m² g⁻¹), their BET surface areas decreased slightly compared with PMO-SO₃H, but the differences in their BET surface areas were negligible. However, the pore volumes of these three samples (1.31, 1.07 and 0.68 m³ g⁻¹) were obviously different, owing to the Si/Zr molar ratio. In the SO₄²⁻/ZrO₂-PMO-SO₃H catalysts, Zr atoms were incorporated into the benzene-bridged organosilica framework through -Zr-O-Si-C₆H₄-Si-O- linkages, whereas SO₄²⁻ anions and -SO₃H groups interacted with the ZrO₂ and phenyl groups, respectively. The incorporation of these two acid sites into a benzene-bridged organosilica framework blocked the pore channels to some extent, which in turn led to the decreased BET surface area and pore volume; moreover, more acid sites were incorporated, resulting in more significant decreases in the BET surface area and pore volume. In the case of SO₄²⁻/ZrO₂-PMO-SO₃H0.25, its much smaller BET surface area (562 m² g⁻¹) and

lower pore volume (0.73 cm³ g⁻¹) originated from the synergistic effect of the structural disordering and high Zr content. The BET surface areas of SO₄²⁻/Nb₂O₅-PMO-SO₃H1.0 (793 m² g⁻¹) and SO₄²⁻/TiO₂-PMO-SO₃H1.0 (700 m² g⁻¹) were smaller than that of SO₄²⁻/ZrO₂-PMO-SO₃H1.0. PF-SO₄²⁻/ZrO₂-PMO-SO₃H1.0 also exhibited a much smaller BET surface area (637 m² g⁻¹) and pore volume (0.56 cm³ g⁻¹).

Composition and structural information

The XPS surface probe technique was applied to study the surface interactions between the SO₄²⁻ anion or -SO₃H group with the ZrO₂-POM framework. Figure 3a shows high-resolution XPS spectra of the ZrO₂ and SO₄²⁻/ZrO₂-PMO-SO₃H1.0 in the Zr 3d binding energy region. The binding energies of Zr 3d_{5/2} and Zr 3d_{3/2} of ZrO₂ were 181.8 and 184.2 eV, respectively, corresponding to the characteristics of the Zr(IV) oxidation state in the ZrO₂. The binding energies of Zr 3d_{5/2} (183.0 eV) and Zr 3d_{3/2} (185.3 eV) shifted to higher values for SO₄²⁻/ZrO₂-PMO-SO₃H1.0, implying a slight perturbation of the zirconium environment due to the interaction between SO₄²⁻ and ZrO₂ as well as the introduction of -Si-C₆H₄-Si- units into the ZrO₂ framework. Similar effects were also observed in the high-resolution XPS spectra of Nb₂O₅ and SO₄²⁻/Nb₂O₅-PMO-SO₃H1.0 in the Nd 3d binding energy region (Figure 3b) as well as TiO₂ and SO₄²⁻/TiO₂-PMO-SO₃H1.0 in the Ti 2p binding energy region (Figure 3c), further confirming the interactions between SO₄²⁻ and Nb₂O₅(TiO₂) as well as the introduction of -Si-C₆H₄-Si- units into the Nb₂O₅(TiO₂) framework.

Figure 3d displays the high-resolution XPS spectra of three bifunctional catalysts in the S 2p binding energy region, which were deconvoluted into two peaks centered at 168.5 and 170.1 eV, corresponding to S 2p_{3/2} and S 2p_{1/2} spin-orbit components, respectively.^[18-20] Therefore, the ZrO₂(Nb₂O₅/TiO₂)-PMO supports were successfully sulfonated by ClSO₃H.

The formation of a benzene-bridged organosilica framework and its subsequent sulfonation were further demonstrated by FT-IR analysis. As shown in Figure 4a, various sulfonated catalysts all exhibited characteristic IR absorption peaks at 1634 as well as 2977 and 2898 cm^{-1} , which were assigned to stretching vibrations of C=C and C-H bonds from the $-\text{Si}-\text{C}_6\text{H}_4-\text{Si}-\text{O}-$ units.^[21] In addition, the peak at 1634 cm^{-1} was possibly due to the stretching vibration of O-H bond from the Si-OH or Zr-OH groups on the surface of the catalysts. The peaks appearing at 3425, 918 as well as 810 and 526 cm^{-1} were attributed to the vibrations of O-H, Si-OH and Si-O-Si bonds, respectively.^[22] Additionally, the other three IR absorption peaks appearing at 1384, 1156 and 1021 cm^{-1} originated from stretching vibrations of S-O and S=O bonds from the $-\text{SO}_3\text{H}$ group and/or SO_4^{2-} anion,^[20,23,24] which suggested that the ZrO_2 -PMO framework was successfully sulfonated by ClSO_3H .

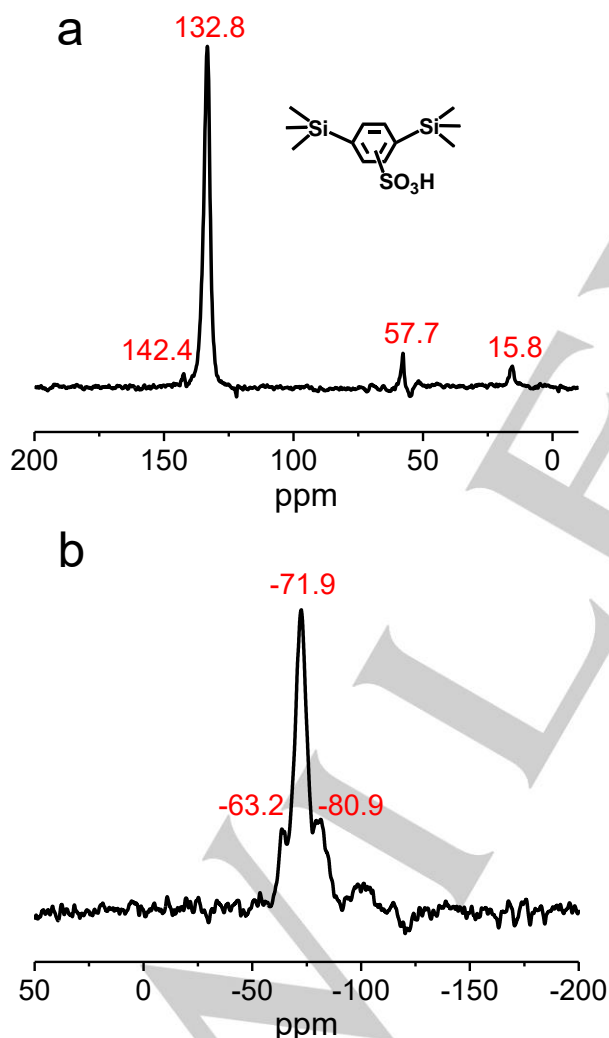


Figure 5. ^{13}C CP (a) and ^{29}Si (b) MAS NMR spectra of the $\text{SO}_4^{2-}/\text{ZrO}_2$ -PMO- $\text{SO}_3\text{H}1.0$.

^{13}C CP-MAS NMR analysis conclusively supported the above result. As shown in Figure 5a, two resonance signals at 132.8 and 142.4 ppm were found in the ^{13}C CP-MAS NMR spectrum of the representative catalyst, $\text{SO}_4^{2-}/\text{ZrO}_2$ -PMO- $\text{SO}_3\text{H}1.0$. The former higher-intensity was attributed to carbon species from the $-\text{Si}-\text{C}_6\text{H}_4-\text{Si}-$ units,^[25] whereas the latter with much weaker intensity was assigned to carbon species from the sulfonated $-\text{Si}-\text{C}_6\text{H}_4-\text{Si}-$ framework.^[26] The other two weak signals at 57.7 and 15.8 ppm were assigned to the carbon species of the ethoxy groups that formed during the boiling ethanol washing process.^[27,28] In the ^{29}Si MAS NMR spectrum of $\text{SO}_4^{2-}/\text{ZrO}_2$ -PMO- $\text{SO}_3\text{H}1.0$ presented in Figure 5b, the characteristic resonances at -63.2 and -71.9 ppm were assigned to organosiloxane species of T^2 [$\text{C}-\text{Si}(\text{OSi})_2(\text{OH})$] and T^3 [$\text{C}-\text{Si}(\text{OSi})_3$],^[29] whereas the resonance signal at -80.9 ppm originated from inorganosiloxane species of Q^1 [$\text{Si}(\text{OSi})(\text{OH})_3$].^[29] These results indicated that not only ZrO_2 but also benzene-bridged organosilica unit can be sulfonated by ClSO_3H during the $\text{SO}_4^{2-}/\text{ZrO}_2$ -PMO- SO_3H preparation process, thereby providing two types of B acid sites, *i.e.*, $\text{SO}_4^{2-}/\text{ZrO}_2$ and PMO- SO_3H (Scheme 1).

Acid nature

The acid site nature of $\text{SO}_4^{2-}/\text{ZrO}_2$ -PMO- SO_3H was characterized by *in situ* pyridine-FT-IR transmission spectroscopy; for comparison, PMO- SO_3H was also tested (Figure 4b). Compared with the FT-IR spectrum of pyridine-free PMO- SO_3H , a new peak at 1593 cm^{-1} was observed in the pyridine-adsorbed FT-IR spectrum of PMO- SO_3H , which was assigned to pyridinium ions formed due to protonation by the $-\text{SO}_3\text{H}$ group.^[30] This result indicated the B acid nature of PMO- SO_3H . The pyridine-adsorbed FT-IR spectra of various $\text{SO}_4^{2-}/\text{ZrO}_2$ -PMO- SO_3H bifunctional catalysts showed three new peaks positioned at 1443, 1489 and 1593 cm^{-1} , respectively, compared with their FT-IR spectra. The peak at 1443 cm^{-1} corresponded to pyridine interacting with L acid sites, *e.g.*, the unsaturated surface Zr^{4+} site of ZrO_2 ,^[31] whereas the peak at 1489 cm^{-1} indicated the co-existence of B and L acid sites in the catalysts. Therefore, the $\text{SO}_4^{2-}/\text{ZrO}_2$ -PMO- SO_3H exhibited both B and L acidity, in which the B acid sites were contributed from both $\text{SO}_4^{2-}/\text{ZrO}_2$ and $-\text{SO}_3\text{H}$ groups confined on the benzene-bridged units. Moreover, the $\text{SO}_4^{2-}/\text{ZrO}_2$ possessed super strong B acidity, and its strong B acidic protons originated from the polarization of surface $-\text{OH}$ groups of ZrO_2 induced by the S=O double bonds of the near sulfate group (Scheme 1).^[32-34]

Similarly, three new peaks at 1443, 1489 and 1593 cm^{-1} were also found in the pyridine-adsorbed FT-IR spectra of $\text{SO}_4^{2-}/\text{Nb}_2\text{O}_5$ -PMO- $\text{SO}_3\text{H}1.0$ and $\text{SO}_4^{2-}/\text{TiO}_2$ -PMO- $\text{SO}_3\text{H}1.0$, suggesting their both B and L acidity. Their B acid sites originated from both $\text{SO}_4^{2-}/\text{Nb}_2\text{O}_5$ (or $\text{SO}_4^{2-}/\text{TiO}_2$) and the $-\text{SO}_3\text{H}$ group, whereas the L acid sites were derived from the unsaturated surface Nb^{5+} (or Ti^{5+}) site of Nb_2O_5 (or TiO_2).

The B acid site density (A_B) of the $\text{SO}_4^{2-}/\text{ZrO}_2$ -PMO- SO_3H was determined by titrating with dilute NaOH solution, whereas the L acid site density (A_L) was calculated based on the n_B/n_L value.^[35] As summarized in Table 1, both B and L acid site densities of

three ordered mesoporous $\text{SO}_4^{2-}/\text{ZrO}_2\text{-PMO-SO}_3\text{H}$ catalysts decreased gradually with increasing Si/Zr molar ratios from 0.5, 1.0 to 2.0, owing to the gradually decreased proportion of the $\text{SO}_4^{2-}/\text{ZrO}_2$ units in the catalysts. For $\text{SO}_4^{2-}/\text{ZrO}_2\text{-PMO-SO}_3\text{H}0.25$, its lower B acid site density compared to $\text{SO}_4^{2-}/\text{ZrO}_2\text{-PMO-SO}_3\text{H}0.5$ was due to its significantly lower BET surface area and thereby decrease in exposed surface acid sites.

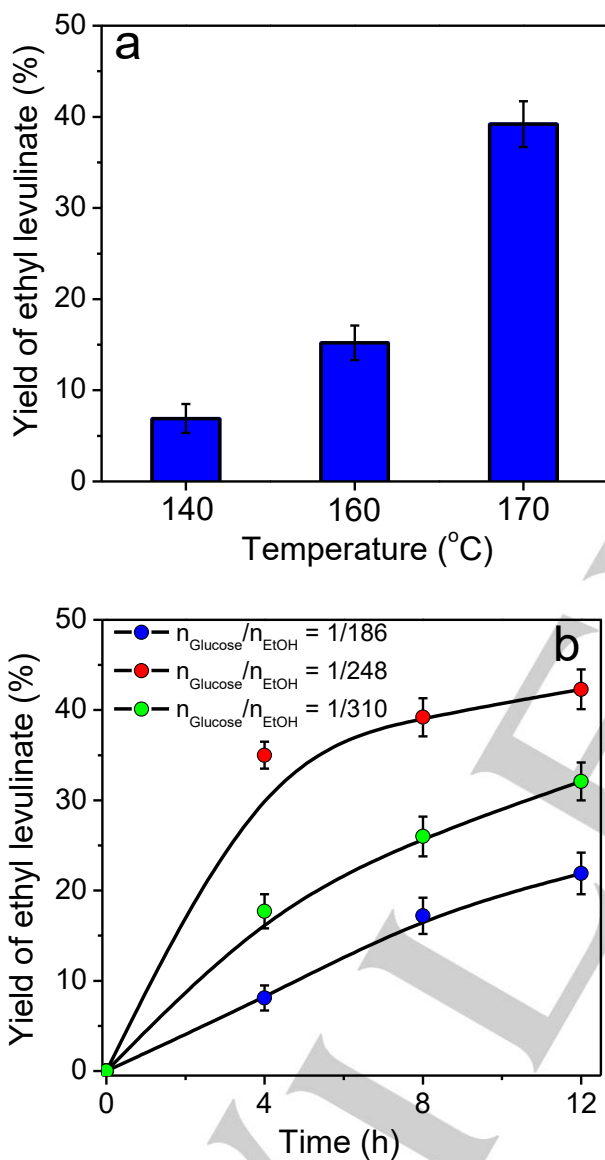


Figure 6. Influence of reaction temperature (a) and glucose-to-ethanol molar ratio ($n_{\text{glucose}}/n_{\text{EtOH}}$) (b) on the catalytic activity of $\text{SO}_4^{2-}/\text{ZrO}_2\text{-PMO-SO}_3\text{H}1.0$ in the conversion of glucose in ethanol. Reaction conditions for Figure 6a: $n_{\text{glucose}}/n_{\text{EtOH}} = 1/248$, 8 h, 1.5 wt% catalyst; reaction conditions for Figure 6b: 170 °C, 1.5 wt% catalyst.

The B and L acid site densities of both $\text{SO}_4^{2-}/\text{Nb}_2\text{O}_5\text{-PMO-SO}_3\text{H}1.0$ and $\text{SO}_4^{2-}/\text{TiO}_2\text{-PMO-SO}_3\text{H}1.0$ were similar to their $\text{SO}_4^{2-}/\text{ZrO}_2\text{-PMO-SO}_3\text{H}1.0$ counterpart; however, the n_B/n_L ratios

of $\text{SO}_4^{2-}/\text{ZrO}_2\text{-PMO-SO}_3\text{H}1.0$, $\text{SO}_4^{2-}/\text{Nb}_2\text{O}_5\text{-PMO-SO}_3\text{H}1.0$ and $\text{SO}_4^{2-}/\text{TiO}_2\text{-PMO-SO}_3\text{H}1.0$ were 0.99, 0.96 and 0.90, respectively, showing that different metal oxides possess different acid capacities.^[32] For $\text{PF-SO}_4^{2-}/\text{ZrO}_2\text{-PMO-SO}_3\text{H}1.0$, its B and L acid site densities (493 and 488 $\mu\text{eq g}^{-1}$) were the lowest because of its worst porosity and thereby the least-exposed acid sites.

Catalytic performance

The catalytic performance of the bifunctional $\text{SO}_4^{2-}/\text{ZrO}_2\text{-PMO-SO}_3\text{H}$ catalysts was evaluated by conversion of glucose to EL in ethanol medium (Scheme 2); reference catalysts including $\text{PMO-SO}_3\text{H}$, $\text{SO}_4^{2-}/\text{ZrO}_2$, $\text{PF-SO}_4^{2-}/\text{ZrO}_2\text{-PMO-SO}_3\text{H}1.0$, $\text{SO}_4^{2-}/\text{ZrO}_2\text{-SiO}_21.0$, $\text{SO}_4^{2-}/\text{Nb}_2\text{O}_5\text{-PMO-SO}_3\text{H}1.0$ and $\text{SO}_4^{2-}/\text{TiO}_2\text{-PMO-SO}_3\text{H}1.0$ as well as commercial HY and H β zeolites were also tested under the same conditions.

Optimization of reaction conditions

The optimization of the reaction temperature was studied by selecting $\text{SO}_4^{2-}/\text{ZrO}_2\text{-PMO-SO}_3\text{H}1.0$ as a representative catalyst. As shown in Figure 6a, the production of EL from conversion of glucose in ethanol medium was significantly accelerated by elevating the reaction temperature from 140, 160 to 170 °C, and the corresponding EL yield reached 6.9, 15.2 and 39.2% after the reaction was performed for 8 h. Therefore, in subsequent catalytic tests, the reaction temperature was set at 170 °C.

Next, the influence of the glucose-to-ethanol molar ratio ($n_{\text{glucose}}/n_{\text{EtOH}}$) on the catalytic activity of the representative $\text{SO}_4^{2-}/\text{ZrO}_2\text{-PMO-SO}_3\text{H}1.0$ was explored at 170 °C. As shown in Figure 6b, over a period of 12 h, the yield of EL reached 21.9, 42.3 and 32.1%, respectively, at $n_{\text{glucose}}/n_{\text{EtOH}}$ ratios of 1/186, 1/248 and 1/310. In the current catalytic system, ethanol was used as both reactant and solvent, and therefore suitable $n_{\text{glucose}}/n_{\text{EtOH}}$ ratio (e.g. 1/248) can facilitate the conversion of glucose to EL; in addition, soluble polymeric humins derived from self-polymerization of the intermediates can be inhibited to some extent.^[36] However, at a lower $n_{\text{glucose}}/n_{\text{EtOH}}$ ratio, e.g. 1/310, the substrate may be diluted, thereby decreasing the EL yield (32.1%); moreover, excessive ethanol may reduce the economic favorability of the above process. Extremely low EL yield (21.9%) was found at a higher $n_{\text{glucose}}/n_{\text{EtOH}}$ ratio (1/186), originating from serious self-polymerization of the intermediates and thereby the decreased selectivity to EL. The above results were consistent with the color changes of the reaction media from light-yellow ($n_{\text{glucose}}/n_{\text{EtOH}}$ ratio of 1/310 and 1/248) to brown-black ($n_{\text{glucose}}/n_{\text{EtOH}}$ ratio of 1/186); in addition, the formed polymeric humins were identified by LC-MS as shown in Figure S2a–e of the SI. Based on these results, an optimum $n_{\text{glucose}}/n_{\text{EtOH}}$ ratio of 1/248 was chosen for subsequent catalytic tests.

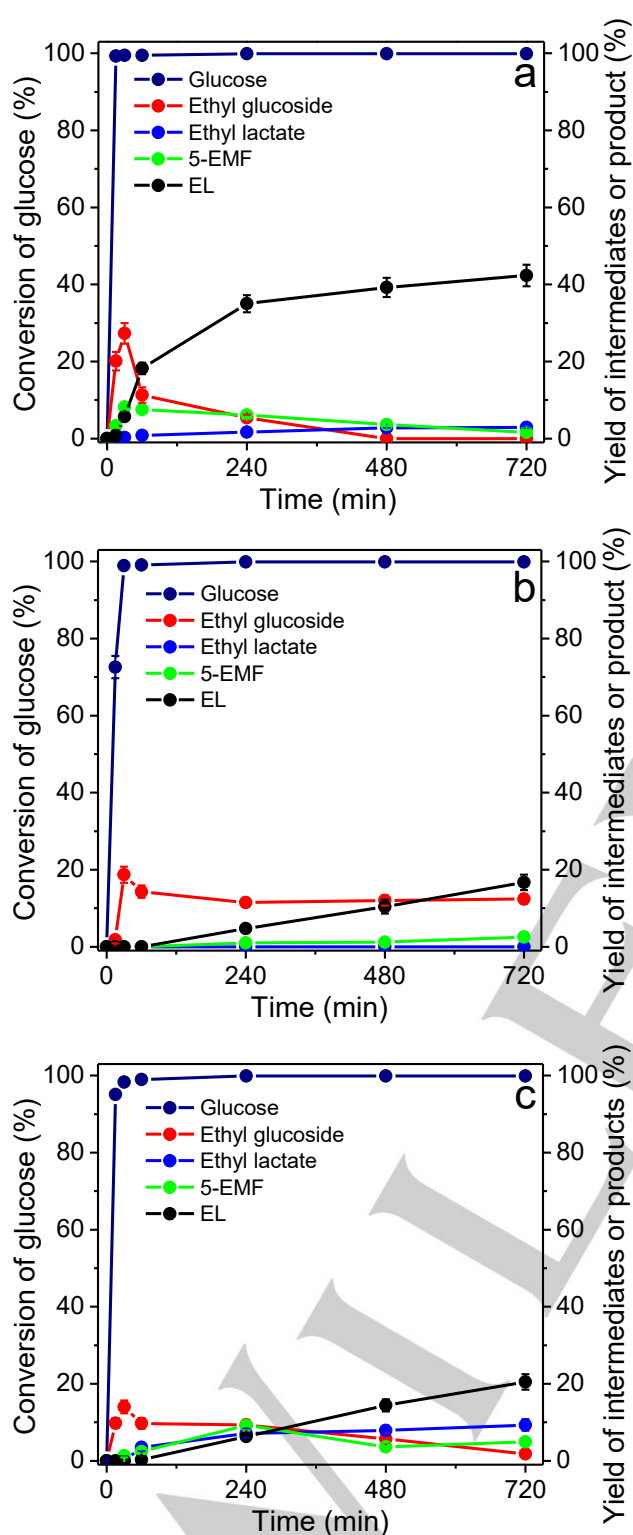


Figure 7. Kinetic studies on conversion of glucose in ethanol over $\text{SO}_4^{2-}/\text{ZrO}_2\text{-PMO-SO}_3\text{H}1.0$ (a), $\text{PMO-SO}_3\text{H}$ (b) and $\text{SO}_4^{2-}/\text{ZrO}_2$ (c). $n_{\text{glucose}}/n_{\text{EtOH}} = 1/248$, 1.5 wt% catalyst, 170 °C.

Reaction pathway and kinetics

As shown in Figure 7, the conversion of glucose in ethanol medium over the bifunctional $\text{SO}_4^{2-}/\text{ZrO}_2\text{-PMO-SO}_3\text{H}1.0$ or monofunctional $\text{PMO-SO}_3\text{H}$ or $\text{SO}_4^{2-}/\text{ZrO}_2$ proceeded rapidly at 170 °C, and glucose conversion was greater than 99% over period of 15 and 30 min, respectively, over the $\text{SO}_4^{2-}/\text{ZrO}_2\text{-PMO-SO}_3\text{H}1.0$ (Figure 7a) and $\text{PMO-SO}_3\text{H}$ (Figure 7b) or $\text{SO}_4^{2-}/\text{ZrO}_2$ (Figure 7c). However, production of the final product EL occurred slowly.

To reveal the contributions of the B and L acid sites of $\text{SO}_4^{2-}/\text{ZrO}_2\text{-PMO-SO}_3\text{H}$ to the formation of EL from glucose, the reaction pathway of the $\text{SO}_4^{2-}/\text{ZrO}_2\text{-PMO-SO}_3\text{H}$ -catalyzed conversion of glucose in ethanol medium was studied by identifying the intermediates and byproducts of the above process *via* both LC-MS and GC-MS; afterwards, kinetic studies were performed by both LC and GC.

Generally, the first step of the synthesis of EL from glucose over bifunctional acid catalysts may experience etherification or isomerization of glucose to ethyl glucoside^[5] or fructose^[9], depending on the acid nature of the catalysts. In the current catalytic system, LC-MS analysis showed that at the initial stage of the reaction (15 min), $\text{SO}_4^{2-}/\text{ZrO}_2\text{-PMO-SO}_3\text{H}1.0$ -catalyzed glucose was mainly transformed into ethyl glucoside (retention time = 8.83 min, $m/z = 206.98$, Figure S3a and c) and ethyl fructoside (retention time = 8.50 min, $m/z = 207.04$, Figure S3a and d). Additionally, trace anhydro monosaccharide byproducts with retention times of 6.48 and 6.80 min were detected (Figure S3a); these byproducts were derived from the dehydration of glucose. After the reaction proceeded for 4 and 12 h, glucose, ethyl glucoside, ethyl fructoside and anhydro monosaccharide disappeared, suggesting that they were further transformed to the intermediates and EL; additionally, the above transformation process was accompanied by the self-polymerization of the intermediates, giving rise to various polymeric humins that were found by LC-MS (Figure S2d and e). GC-MS analysis indicated that the intermediate 5-EMF (retention time = 9.30 min), byproduct ethyl lactate (retention time = 6.97 min) and final product EL (retention time = 10.97 min) were identified at a reaction time of 8 h (Figure S4). However, fructose was not detected in this system.

The above results indicate that the production of EL from the $\text{SO}_4^{2-}/\text{ZrO}_2\text{-PMO-SO}_3\text{H}$ -catalyzed conversion of glucose in ethanol medium followed the reaction pathway of glucose–ethyl glucoside–ethyl fructoside–5-EMF–EL *via* successive etherification, isomerization, dehydration and ring-opening steps, which were dominated by the synergistic effect of the super strong B acidity and moderate L acidity of the $\text{SO}_4^{2-}/\text{ZrO}_2\text{-PMO-SO}_3\text{H}$.^[5,9,37,38] In detail, as illustrated in Scheme 2, the super strong B acid sites ($\text{SO}_4^{2-}/\text{ZrO}_2$ and $-\text{SO}_3\text{H}$) of $\text{SO}_4^{2-}/\text{ZrO}_2\text{-PMO-SO}_3\text{H}$ can activate the hemiacetal hydroxy of glucose first, and the activated glucose is then attacked by ethanol to produce ethyl glucoside and water *via* an etherification reaction. Subsequently, the L acid sites (Zr^{4+}) of the bifunctional catalysts facilitate the breakage of the C–O bond of the six-membered ring structured ethyl glucoside, followed by ring-opening and isomerization to generate ethyl fructoside. Next, ethyl fructoside

undergoes dehydration and breakage of C–O bonds with the assistance of the B acid sites to produce 5-EMF. Finally, protonation of 5-EMF by the B acid sites gives rise to cyclic oxonium, and EL is produced by a ring-opening reaction of the cyclic oxonium under attack by water and ethanol. Therefore, in the bifunctional $\text{SO}_4^{2-}/\text{ZrO}_2\text{-PMO-SO}_3\text{H}$ catalytic system, super strong B acidity and double B acid sites are responsible for etherification of glucose to ethyl glucoside in the first step of glucose conversion, whereas the moderate L acid sites of the catalyst are active for the isomerization of ethyl glucoside to ethyl fructoside; subsequent dehydration of ethyl glucoside to 5-EMF and then ring-opening of the activated 5-EMF to EL are catalyzed by the B acid sites of the catalysts.

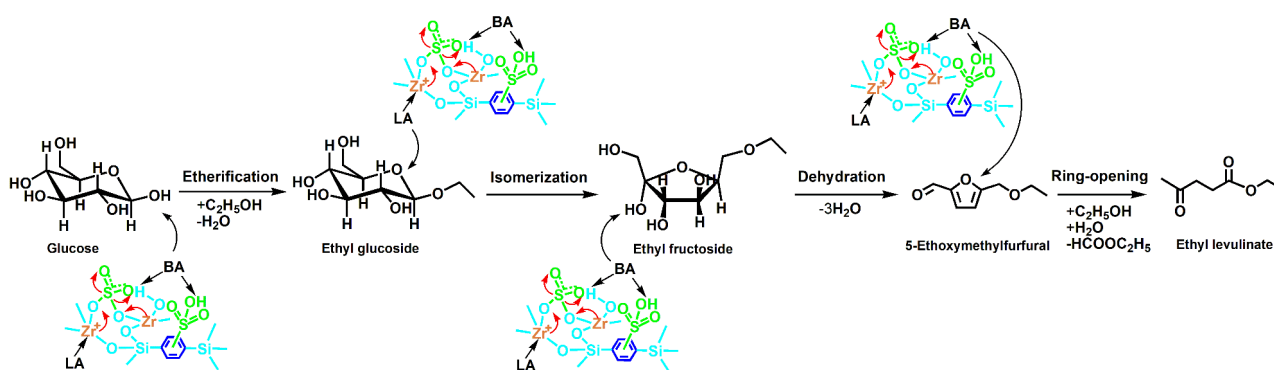
On the basis of the above results, kinetic studies of $\text{SO}_4^{2-}/\text{ZrO}_2\text{-PMO-SO}_3\text{H1.0}$ -, $\text{PMO-SO}_3\text{H}$ - and $\text{SO}_4^{2-}/\text{ZrO}_2$ -catalyzed conversion of glucose to ethyl glucoside, 5-EMF, ethyl lactate and EL in ethanol medium were performed. As shown in Figure 7a, at the initial stage of the $\text{SO}_4^{2-}/\text{ZrO}_2\text{-PMO-SO}_3\text{H1.0}$ -catalyzed glucose conversion reaction, the yield of ethyl glucoside increased gradually, and the highest yield of ethyl glucoside (27.3%) was obtained after the reaction proceeded for 30 min. As the reaction time was further prolonged, the yield of ethyl glucoside decreased quickly and disappeared over a period of 480 min. This result implies that ethyl glucoside was transformed to ethyl fructoside and other intermediates rapidly, a prerequisite for ensuring the production of EL with considerably high yield. The highest 5-EMF yield of 8.2% was obtained at 30 min, and the yield decreased gradually with increasing reaction time. The total yields of all detected intermediates were less than 2% after the reaction was performed for 720 min, suggesting that they were further converted to the final product EL and polymeric humins. Additionally, only a small amount of ethyl lactate (2.9%) was obtained in the current catalytic system. Formation of ethyl lactate was catalyzed by the L acid sites of the catalysts *via* retro-aldol reaction followed by isomerization, which competed with the dehydration of 5-EMF catalyzed by the B acid sites.^[15] Since $\text{SO}_4^{2-}/\text{ZrO}_2\text{-PMO-SO}_3\text{H}$ exhibited moderate L acid sites, the production of ethyl lactate in glucose conversion was obviously inhibited, which was favorable for the production of EL with high yield. Consequently, $\text{SO}_4^{2-}/\text{ZrO}_2\text{-PMO-SO}_3\text{H1.0}$ exhibited a relatively high EL yield compared with reported catalytic systems.^[5,7,37] For example, after the reaction time proceeded for 720 min, the EL yield reached 42.3%. However, for the reported $\text{SO}_4^{2-}/\text{ZrO}_2$ -catalyzed ethanolysis of glucose, the EL yield was *ca.* 30% under the conditions of catalyst dosage of 2.5 wt%, 200 °C and 3 h;^[37] in addition, in the reported sulfated zirconia grafted SBA-15-catalyzed reaction of glucose with ethanol, the EL yield of *ca.* 25% was obtained at 140 °C and 24 h.^[5] The formation of polymeric humins due to self-polymerization of the intermediates during the glucose conversion process accounted for significant carbon loss of the feed, causing limited EL yield in the present and reported catalytic systems (Figure S2f-h).^[39]

In order to further evaluate the catalytic activity of $\text{SO}_4^{2-}/\text{ZrO}_2\text{-PMO-SO}_3\text{H}$, as-prepared $\text{PMO-SO}_3\text{H}$ and $\text{SO}_4^{2-}/\text{ZrO}_2$ were also tested under the same conditions. As displayed in Figure 7b, the yield of ethyl glucoside reached the maximum value of 18.7% as

the $\text{PMO-SO}_3\text{H}$ -catalyzed glucose conversion reaction proceeded for 30 min. However, in contrast to bifunctional $\text{SO}_4^{2-}/\text{ZrO}_2\text{-PMO-SO}_3\text{H1.0}$, when the reaction time was continuously increased to 720 min, ethyl glucoside remained in the $\text{PMO-SO}_3\text{H}$ system with a yield of 12.4%. Additionally, only trace 5-EMF yielded, and the maximum 5-EMF yield of 2.5% was obtained after the reaction was performed for 720 min. Ethyl lactate was not produced in this system. $\text{PMO-SO}_3\text{H}$ only had B acid sites, and in the $\text{PMO-SO}_3\text{H}$ -catalyzed glucose conversion process, glucose was etherified to ethyl glucoside. However, owing to the weaker B acid strength of $\text{PMO-SO}_3\text{H}$ compared with $\text{SO}_4^{2-}/\text{ZrO}_2\text{-PMO-SO}_3\text{H1.0}$, the yield of ethyl glucoside was lower over $\text{PMO-SO}_3\text{H}$. In addition, owing to the absence of L acid sites, it was difficult to further isomerize ethyl glucoside to ethyl fructoside. Accordingly, ethyl glucoside still remained in the system with considerably high yield, which significantly limited further conversion of ethyl fructoside to 5-EMF and EL. Accordingly, the EL yield (16.7%, 720 min) over $\text{PMO-SO}_3\text{H}$ was obviously lower than that over $\text{SO}_4^{2-}/\text{ZrO}_2\text{-PMO-SO}_3\text{H1.0}$. Additionally, the pure B acid nature of the $\text{PMO-SO}_3\text{H}$ prevented the formation of ethyl lactate.

Although $\text{SO}_4^{2-}/\text{ZrO}_2$ exhibited both B and L acid nature, it catalyzed the glucose conversion reaction with lower EL yield (20.5%, 720 min) compared with $\text{SO}_4^{2-}/\text{ZrO}_2\text{-PMO-SO}_3\text{H1.0}$ (Figure 7c). This result is due to its single B acid sites as well as very small BET surface area ($12\text{ m}^2\text{ g}^{-1}$).^[32] Additionally, the yield of ethyl glucoside reached 14.0% at 30 min and then decreased to 1.8% at 720 min with the aid of L acid sites. The highest 5-EMF yield of 9.2% was obtained at 240 min, and the yield decreased to 4.9% at 720 min.

Subsequently, the catalytic activities of the bifunctional $\text{SO}_4^{2-}/\text{ZrO}_2\text{-PMO-SO}_3\text{H}$ catalysts prepared at Si/Zr molar ratios of 0.25, 0.5, 1.0 and 2.0 were compared in conversion of glucose to EL. As shown in Figure 8a, $\text{SO}_4^{2-}/\text{ZrO}_2\text{-PMO-SO}_3\text{H1.0}$ was the most active in the target reaction, whereas the catalytic activities of $\text{SO}_4^{2-}/\text{ZrO}_2\text{-PMO-SO}_3\text{H0.25}$ and $\text{SO}_4^{2-}/\text{ZrO}_2\text{-PMO-SO}_3\text{H2.0}$ were similar and both the lowest. After the $\text{SO}_4^{2-}/\text{ZrO}_2\text{-PMO-SO}_3\text{H0.25}$ -, $\text{SO}_4^{2-}/\text{ZrO}_2\text{-PMO-SO}_3\text{H0.5}$ -, $\text{SO}_4^{2-}/\text{ZrO}_2\text{-PMO-SO}_3\text{H1.0}$ - and $\text{SO}_4^{2-}/\text{ZrO}_2\text{-PMO-SO}_3\text{H2.0}$ -catalyzed glucose conversion reactions proceeded for 12 h, the yield of EL was 20.6, 30.5, 42.3 and 21.5%, respectively. The above results can be explained by the influence of the initial Si/Zr molar ratios on the porosity properties, the acid site densities of B and L acid and the B-to-L acid molar ratio. All of these factors were important influences on the catalytic activity of $\text{SO}_4^{2-}/\text{ZrO}_2\text{-PMO-SO}_3\text{H}$. $\text{SO}_4^{2-}/\text{ZrO}_2\text{-PMO-SO}_3\text{H2.0}$ possessed perfect porosity properties, including the largest BET surface area ($959\text{ m}^2\text{ g}^{-1}$) and pore size (6.4 nm) as well as the highest pore volume ($1.31\text{ cm}^3\text{ g}^{-1}$), among four bifunctional $\text{SO}_4^{2-}/\text{ZrO}_2\text{-PMO-SO}_3\text{H}$ catalysts, and its poor catalytic activity in the target reaction was due to the lowest acid site density of B and L acids. $\text{SO}_4^{2-}/\text{ZrO}_2\text{-PMO-SO}_3\text{H0.25}$ had a considerably high acid site density of B and L acids, and its poor catalytic activity originated from its inferior porosity properties and the highest n_B/n_L ratio. $\text{SO}_4^{2-}/\text{ZrO}_2\text{-PMO-SO}_3\text{H0.5}$ had the highest acid site densities of B and L acids, and its BET surface area remained sufficiently large.



Scheme 2. Reaction pathway of the $\text{SO}_4^{2-}/\text{ZrO}_2\text{-PMO-SO}_3\text{H}$ -catalyzed conversion of glucose to ethyl levulinate in ethanol medium.

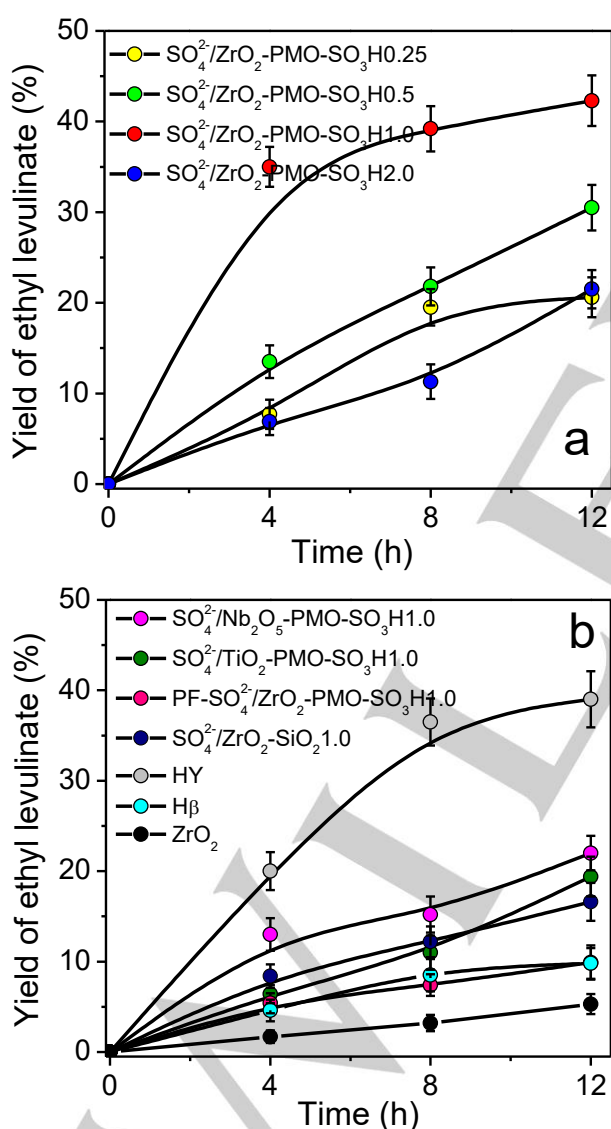


Figure 8. Catalytic activity comparison of various $\text{SO}_4^{2-}/\text{ZrO}_2\text{-PMO-SO}_3\text{H}$ catalysts (a) and reference solid acids (b) in the conversion of glucose to ethyl levulinate. $n_{\text{glucose}}/n_{\text{EtOH}} = 1/248$, 1.5 wt% catalyst, 170 °C.

Its lower activity compared to the most active catalyst, $\text{SO}_4^{2-}/\text{ZrO}_2\text{-PMO-SO}_3\text{H}1.0$ was due to its smaller pore diameter, lower pore volume and higher n_B/n_L ratio. Therefore, based on the combination of its advantages of considerably high acid site densities of B and L acids, the lowest n_B/n_L ratio and excellent porosity properties, $\text{SO}_4^{2-}/\text{ZrO}_2\text{-PMO-SO}_3\text{H}1.0$ exhibited the highest catalytic activity in the conversion of glucose to EL. A high n_L/n_B ratio can accelerate the isomerization of ethyl glucoside to ethyl fructoside, one of the key steps for the conversion of glucose to EL. Additionally, well-ordered mesostructures of the catalyst can facilitate mass transfer and diffusion of the reactants to the acid sites, whereas a large BET surface and high pore volume can provide a high population of acid sites. Importantly, $\text{SO}_4^{2-}/\text{ZrO}_2\text{-PMO-SO}_3\text{H}1.0$ possessed a larger pore diameter (5.5 nm), which can accommodate bulky glucose and its intermediates in reactions in the mesopores. All of the above factors led to the increased accessibility of the reactants to the acid sites and thereby enhanced catalytic activity in the conversion of glucose to EL.

Figure 8b presents the catalytic activity of various reference catalysts in the target reaction. All were less active than $\text{SO}_4^{2-}/\text{ZrO}_2\text{-PMO-SO}_3\text{H}1.0$. Over a period of 12 h, the yield of EL reached 39.0, 16.6, 9.9, 9.8 and 5.3% in the HY-, $\text{SO}_4^{2-}/\text{ZrO}_2\text{-SiO}_2\text{1.0-}$, PF- $\text{SO}_4^{2-}/\text{ZrO}_2\text{-PMO-SO}_3\text{H}1.0\text{-}$, H β - and ZrO $_2$ -catalyzed target reaction; additionally, in the same reaction time, the yield of EL was 22.0 and 19.4% for the $\text{SO}_4^{2-}/\text{Nb}_2\text{O}_5\text{-PMO-SO}_3\text{H}1.0\text{-}$ and $\text{SO}_4^{2-}/\text{TiO}_2\text{-PMO-SO}_3\text{H}1.0\text{-}$ -catalyzed target reactions. The obviously lower catalytic activity of PF- $\text{SO}_4^{2-}/\text{ZrO}_2\text{-PMO-SO}_3\text{H}1.0$ compared to its $\text{SO}_4^{2-}/\text{ZrO}_2\text{-PMO-SO}_3\text{H}1.0$ counterpart is due to its disordered mesostructure, which led to poor porosity properties as well as low acid site densities of B and L acids. Similarly, the lower catalytic activity of $\text{SO}_4^{2-}/\text{Nb}_2\text{O}_5\text{-PMO-SO}_3\text{H}1.0$ or $\text{SO}_4^{2-}/\text{TiO}_2\text{-PMO-SO}_3\text{H}1.0$ than its $\text{SO}_4^{2-}/\text{ZrO}_2\text{-PMO-SO}_3\text{H}1.0$ counterpart is also due to its obviously decreased BET surface area and acid site density of B and L acids. The lower catalytic activity of HY zeolite compared to $\text{SO}_4^{2-}/\text{ZrO}_2\text{-PMO-SO}_3\text{H}1.0$ is mainly due to its smaller BET surface area (700 m 2 g $^{-1}$, Table 1) and pore diameter (2.5 nm), which can reduce the accessibility of the substrates to acid sites.

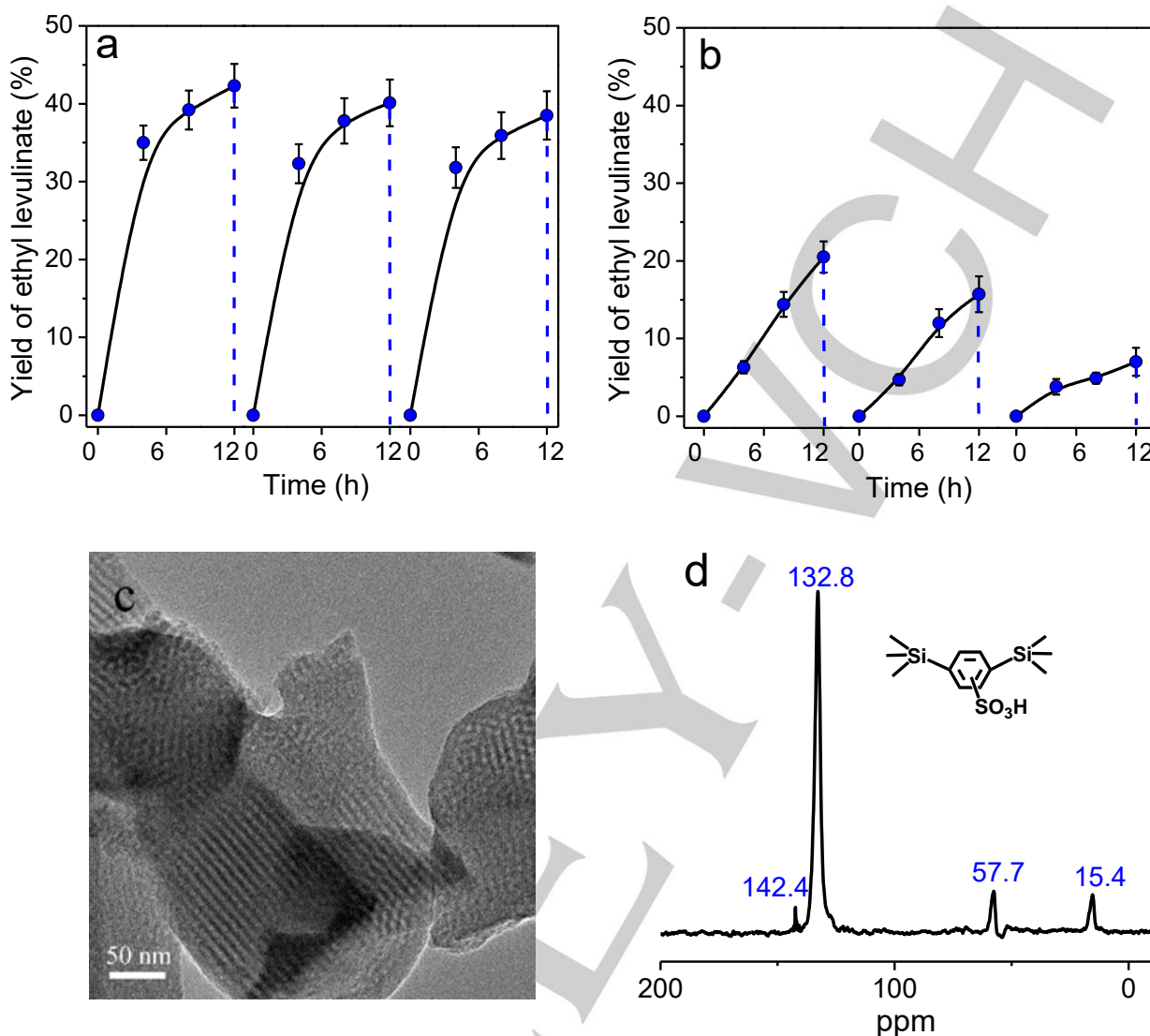


Figure 9. Reusability of SO₄²⁻/ZrO₂-PMO-SO₃H1.0 (a) and SO₄²⁻/ZrO₂ (b) in the conversion of glucose to ethyl levulinate. $n_{\text{glucose}}/n_{\text{EtOH}} = 1/248$; 1.5 wt% catalyst, 170 °C, 12 h. TEM image (c) and ¹³C CP MAS NMR (d) of the third time spent SO₄²⁻/ZrO₂-PMO-SO₃H1.0 catalyst.

The microporous H β zeolite with a pore diameter of 0.7 nm limits the accessibility of bulky reactant molecules to the acid sites, thereby severely hindering diffusion and resulting in poor ethanolysis activity. The lower catalytic activity of SO₄²⁻/ZrO₂-SiO₂1.0 is due to the following two factors. One, owing to the lack of bridging benzene groups in the silica framework, the porosity properties of SO₄²⁻/ZrO₂-SiO₂1.0 (BET surface area of 314 m² g⁻¹, pore diameter of 4.2 nm and pore volume of 0.72 cm³ g⁻¹, Table 1) were inferior to those of SO₄²⁻/ZrO₂-PMO-SO₃H1.0, which may limit the accessibility of the reactants to the acid sites. Second, the SO₄²⁻/ZrO₂-SiO₂1.0 had single (*i.e.*, SO₄²⁻/ZrO₂) rather than double B acid sites; accordingly, its B acid site density (545 $\mu\text{eq g}^{-1}$) was lower than that of SO₄²⁻/ZrO₂-PMO-SO₃H1.0, which may lead to a slower reaction rate in

the conversion of glucose to EL compared with SO₄²⁻/ZrO₂-PMO-SO₃H1.0.

The surface hydrophobicity of the SO₄²⁻/ZrO₂-PMO-SO₃H catalysts due to incorporation of Si(C₆H₄)Si units into ZrO₂ framework also positively influenced their catalytic activity in the target reaction, thereby effectively reducing the adsorption of hydrophilic byproducts such as ethyl lactate, anhydro monosaccharide and polymeric humins on the catalyst surface.^[40] However, these products may strongly adsorb on the SO₄²⁻/ZrO₂ surface because of its surface hydrophilicity, leading to decreased accessibility of the acid sites.

Regeneration and reusability

Catalytic stability and reusability are significant challenges for practical applications of bifunctional $\text{SO}_4^{2-}/\text{ZrO}_2\text{-PMO-SO}_3\text{H}$ in the conversion of glucose to EL. Here, the stability and reusability of as-prepared catalysts were evaluated by recycling $\text{SO}_4^{2-}/\text{ZrO}_2\text{-PMO-SO}_3\text{H}$ 1.0 three times. After each catalytic cycle, the spent catalyst was recovered by centrifugation, followed by thorough ethanol washing before the second and third catalytic cycles. For comparison, the reusability of $\text{SO}_4^{2-}/\text{ZrO}_2$ was also tested under the same conditions. As shown in Figure 9a, after the $\text{SO}_4^{2-}/\text{ZrO}_2\text{-PMO-SO}_3\text{H}$ 1.0-catalyzed glucose conversion reaction was performed for 12 h, the yield of EL was 42.3 (1st cycle), 40.1 (2nd cycle) and 38.5% (3rd cycle), respectively. This result indicated that the $\text{SO}_4^{2-}/\text{ZrO}_2\text{-PMO-SO}_3\text{H}$ can be reused three times without obvious activity loss. However, for the $\text{SO}_4^{2-}/\text{ZrO}_2$ -catalyzed target reaction, the yield of EL decreased clearly from 20.5 (1st cycle), 15.7 (2nd cycle) to 7.0% (3rd cycle), after the reaction performed for 12 h (Figure 9b). $\text{SO}_4^{2-}/\text{ZrO}_2$, which has plentiful Zr-OH groups, exhibits a hydrophilic surface, that can strongly adsorb hydrophilic humins, resulting in deactivation of $\text{SO}_4^{2-}/\text{ZrO}_2$ during its recycling runs.

To support the above results, TEM image and ^{13}C CP MAS NMR of the third time spent $\text{SO}_4^{2-}/\text{ZrO}_2\text{-PMO-SO}_3\text{H}$ 1.0 catalyst were measured. As shown in Figure 9c, the spent $\text{SO}_4^{2-}/\text{ZrO}_2\text{-PMO-SO}_3\text{H}$ 1.0 still exhibited a perfect 2D hexagonal mesostructure, implying its excellent mechanical stability and resistance to byproduct adsorption. These properties ensured the excellent reusability of $\text{SO}_4^{2-}/\text{ZrO}_2\text{-PMO-SO}_3\text{H}$.

^{13}C CP-MAS NMR of the spent $\text{SO}_4^{2-}/\text{ZrO}_2\text{-PMO-SO}_3\text{H}$ revealed all characteristic signals for various carbon species in $\text{SO}_4^{2-}/\text{ZrO}_2\text{-PMO-SO}_3\text{H}$, the carbon species of the bridging benzene units (132.8 ppm) and $-\text{SO}_3\text{H}$ functionalized benzene groups (142.4 ppm) are shown in Figure 9d. Additionally, signals still appeared at 57.7 and 15.8 ppm, owing to the carbon species of the ethoxy group that formed during the boiling ethanol washing process.^[27,28] This result suggested that the Si-C framework remains intact after the catalytic cycles; more importantly, byproducts were hardly found on the surface of the spent catalyst. The excellent reusability of $\text{SO}_4^{2-}/\text{ZrO}_2\text{-PMO-SO}_3\text{H}$ is mainly due to the strong covalent bonding between double B acid sites and the $\text{ZrO}_2\text{-PMO}$ framework; in addition, the surface hydrophobicity of the catalysts can effectively avoid catalyst deactivation, owing to byproduct adsorption. Therefore, the $\text{SO}_4^{2-}/\text{ZrO}_2\text{-PMO-SO}_3\text{H}$ catalysts are promising alternatives to hazardous liquid acids employed in effective conversion of glucose directly to EL.

Conclusions

A series of bifunctional $\text{SO}_4^{2-}/\text{ZrO}_2\text{-PMO-SO}_3\text{H}$ catalysts with both B and L acid sites were successfully prepared by a carefully designed sol-gel co-condensation route followed by ClSO_3H functionalization. The acid site density, structural ordering and porosity properties of $\text{SO}_4^{2-}/\text{ZrO}_2\text{-PMO-SO}_3\text{H}$ were optimally tuned by adjusting the initial Si/Zr molar ratios to 0.25, 0.5, 1.0 and 2.5. Owing to the synergistic effect of the super strong B acidity and moderate L acidity of the bifunctional

catalysts, $\text{SO}_4^{2-}/\text{ZrO}_2\text{-PMO-SO}_3\text{H}$ -catalyzed the conversion of glucose to EL followed by etherification of glucose with ethanol as the first step. Additionally, the $\text{SO}_4^{2-}/\text{ZrO}_2\text{-PMO-SO}_3\text{H}$ catalyst prepared at a Si/Zr molar ratio of 1.0 exhibited the highest EL yield (42.3%) among various as-prepared catalysts, and its catalytic activity outperformed HY (EL yield of 39.0%) and H β (EL yield of 9.8%) zeolites. The acid site densities of B and L acids, the molar ratio of B-to-L acid sites, structural ordering and porosity properties gave the important influence on the catalytic activity of the bifunctional $\text{SO}_4^{2-}/\text{ZrO}_2\text{-PMO-SO}_3\text{H}$ in the target reaction. Moreover, the catalysts exhibited excellent reusability, which was attributed to the strong covalent bonding between double B acid sites and the $\text{ZrO}_2\text{-PMO}$ framework; in addition, the surface hydrophobicity of the catalysts can effectively avoid catalyst deactivation, owing to byproduct adsorption. Therefore, the $\text{SO}_4^{2-}/\text{ZrO}_2\text{-PMO-SO}_3\text{H}$ catalysts are promising alternatives to hazardous liquid acids employed in the effective conversion of glucose directly to EL.

Experimental Section

Materials

Pluronic P123 ($\text{EO}_{20}\text{PO}_{70}\text{EO}_{20}$, EO = $-\text{CH}_2\text{CH}_2\text{O}-$, PO = $-\text{CH}_2(\text{CH}_3)\text{CHO}-$), 1,4-bis-(triethoxysilyl)benzene (BTESB, 96%), zirconium *n*-butoxide [$\text{Zr}(\text{O}n\text{Bu})_4$, 76–80% in *n*-butanol], NbCl_5 (> 99%), titanium *iso*-propylate (TTIP, 97%) and 5-ethoxymethylfurfural (5-EMF, > 97%) were purchased from Sigma-Aldrich. Ethyl levulinate (EL, > 98%), chlorosulfonic acid (ClSO_3H , > 97%) and ethyl laurate (> 99%) were purchased from TCI. Ethyl lactate (> 99%) was purchased from J&K Scientific. Ethyl- β -D-glucoside (> 95%) was purchased from Aikon. Y and beta zeolite powders were purchased from Nankai University Catalyst Co. NH_4 -form zeolites were obtained by ion-exchange twice with NH_4NO_3 solution (0.5 mol L^{-1}) at 80 °C for 2 h, and protonic form zeolites were obtained by calcination of the NH_4 -zeolites at 550 °C for 5 h.

Catalytic preparation

Typically, P123 (0.275 g) was dissolved in a mixture of HCl (12 mol L^{-1} , 0.6 mL) and distilled water (8.5 mL) at room temperature under stirring. The obtained P123 solution was heated to 40 °C, and then BTESB (0.68 mL) was added. After prehydrolysis of BTESB for 45 min, $\text{Zr}(\text{O}n\text{Bu})_4$ (3.0, 1.5, 0.75 or 0.375 mL to adjust the Si/Zr molar ratio to 2.0, 1.0, 0.5 or 0.25, respectively) was added to the above mixture. The resultant white suspension was stirred at 40 °C for 24 h. The suspension was transferred to an autoclave and heated to 120 °C at a heating rate of 2 °C min^{-1} , and then it was held at this temperature for another 24 h. The resulting white solid powder was air-dried at 60, 80 and 100 °C, respectively, for 12 h. P123 in the product was removed by washing three times with boiling ethanol, and the mesostructured ZrO_2 -organosilica support ($\text{ZrO}_2\text{-PMO}$) was obtained after air drying at 100 °C overnight.

Subsequently, $\text{ZrO}_2\text{-PMO}$ powder (0.5 g) was dispersed into a mixture of ClSO_3H (5 mL) and dichloromethane (25 mL), and the obtained suspension was stirred at 0 °C for 12 h under argon gas. In the above process, ClSO_3H was in excess with respect to the total moles of Si and Zr. Finally, the suspension was washed with copious amounts of water until the filtrate was neutral. After centrifugation and washing with ethanol, the powder product was dried at 100 °C overnight. The initial molar ratio of the reactants was P123: BTESB: $\text{Zr}(\text{O}n\text{Bu})_4$: ClSO_3H : HCl: H_2O = 0.029: 1: (0.25, 0.5, 1 or 2): 45: 4.4: 288. The product was denoted as

$\text{SO}_4^{2-}/\text{ZrO}_2\text{-PMO-SO}_3\text{H}_x$, where x represents the initial Si/Zr molar ratio; here, $x = 0.25, 0.5, 1.0$ and 2.0 .

$\text{PMO-SO}_3\text{H}$ and $\text{PF-SO}_4^{2-}/\text{ZrO}_2\text{-PMO-SO}_3\text{H}1.0$ were prepared based on the above procedure but in the absence of $\text{Zr}(\text{O}i\text{Bu})_4$ or P123, respectively.

Ordered mesoporous silica functionalized by sulfonic acid and ZrO_2 ($\text{SO}_4^{2-}/\text{ZrO}_2\text{-SiO}_21.0$) was prepared following a route of similar to that for $\text{SO}_4^{2-}/\text{ZrO}_2\text{-PMO-SO}_3\text{H}1.0$ except that TEOS was used as the silicon precursor instead of BTESB.

$\text{SO}_4^{2-}/\text{Nb}_2\text{O}_5\text{-PMO-SO}_3\text{H}1.0$ and $\text{SO}_4^{2-}/\text{TiO}_2\text{-PMO-SO}_3\text{H}1.0$ were prepared based on the above procedure except that NbCl_5 and TTIP, respectively, were used as the precursors instead of $\text{Zr}(\text{O}i\text{Bu})_4$.

Catalyst characterization

TEM observations were performed on a JEM-2100F high resolution transmission electron microscope at an accelerating voltage of 200 kV. Small angle X-ray scattering (SAXS) patterns were obtained on a D/max-2200 VPC diffractometer using $\text{CuK}\alpha$ radiation. Nitrogen porosimetry measurements were performed on a Micromeritics ASAP 2020M surface area and porosity analyzer after the samples were outgassed under vacuum at 363 K for 1 h and 393 K for 6 h. XPS was performed on a VG-ADES 400 instrument with a Mg $\text{K}\alpha$ -ADES source at a residual gas pressure of less than 10^{-8} Pa. All binding energies were referenced to the C 1s peak at 284.8 eV of the surface adventitious carbon. FT-IR spectra in transmission mode were recorded on a Nicolet Magna 560 IR spectrophotometer, and the catalyst powder samples were first admixed with KBr and then pressed into the pellets. ^{13}C CP-MAS and ^{29}Si MAS NMR spectra were recorded on a Bruker AVANCE III 400 WB spectrometer equipped with a 4 mm standard bore CP MAS probe head. Chemical shifts for ^{13}C CP-MAS NMR and ^{29}Si MAS NMR spectra were referenced to the signals of a $\text{C}_{10}\text{H}_{16}$ standard ($\delta_{\text{CH}_2} = 38.5$) and 3-(trimethylsilyl)-1-propanesulfonic acid sodium salt standard ($\delta = 0.0$), respectively.

The nature of the acid sites was distinguished by *in situ* FT-IR spectroscopy with chemical adsorption of pyridine. Before the determination, the samples were pretreated at 100 °C for 12 h in a vacuum. The samples were then exposed to pyridine vapor at 60 °C for 12 h in a vacuum, followed by pumping out at 150 °C for 1 h to remove the physisorbed pyridine.

L and B acid sites were quantified by integrating the area underneath the bands at 1450 and 1540 cm^{-1} , respectively,^[35] and the corresponding molar ratio of B-to-L acid was then estimated.

The B acid site density was determined by titration. Typically, fresh catalyst powder (50 mg) was dispersed in a NaCl solution (2 mol L^{-1} , 10 mL) under stirring at 30 °C for 24 h, and then the suspension was titrated with standard NaOH solution (4.6 mmol L^{-1}).^[41] The B acid site density ($\mu\text{eq g}^{-1}$) was calculated from the consumed NaOH, whereas the L acid-site density was calculated based on molar ratio of B-to-L acid (n_B/n_L) and the B acid site density.

Catalytic tests

Catalyst powders were dried for 2 h at 120 °C under vacuum before the tests. Conversion of glucose to EL was conducted in an autoclave with a Teflon lining at 170 °C, a glucose (0.278 mmol) to ethanol (68.95 mmol) molar ratio of 1:248 and 50 mg or 1.5 wt% catalyst (with respect to total reactants); stirring was applied throughout the reaction. Conversion of glucose and the yield of ethyl glucoside were determined on an Agilent 1260HPLC liquid chromatograph fitted with an ACQUITY UPLC Prevalil Carbohydrate column (film thickness, 5 μm ; *i.d.*, 4.6 mm; length, 250 mm) and an evaporative light-scattering detector (Alltech ELSD 2000ES). The flow rate of the mobile phase (acetonitrile: water = 85: 15) was 1 mL min^{-1} . The operation conditions of the detector were a tube temperature

of 105 °C; and a gas flow rate of 2.3 L min^{-1} . The concentrations of EL, 5-EMF and ethyl lactate were determined periodically on a Shimadzu 2014C gas chromatograph fitted with an HP-INNOWAX capillary column (film thickness, 0.5 μm ; *i.d.*, 0.32 mm; length, 30 m) and flame ionization detector, and ethyl laurate was applied as an internal standard. The intermediates and byproducts obtained during the catalytic processes were identified by both GC-MS (HP6890GC-5973MSD) and LC-MS (Thermo Scientific LTQ-Orbitrap XL).

Acknowledgements ((optional))

This work is supported by the Natural Science Fund Council of China (21573038 and 21703030) and the Fundamental Research Funds for the Central Universities (130014725).

Keywords: biomass • glucose • ethyl levulinate • solid acid • Brønsted and Lewis acid

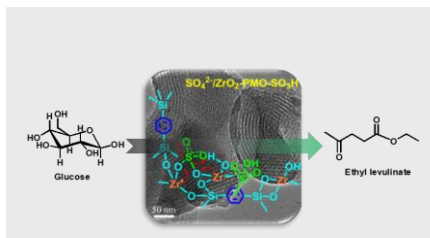
- [1] L. Yan, Q. Yao and Y. Fu, *Green Chem.* **2017**, *19*, 5527-5547.
- [2] K. Jacobson, R. Gopinath, L. C. Meher and A. K. Dalai, *Appl. Catal. B: Environ.* **2008**, *85*, 86-91.
- [3] A. Sivasamy, K. Y. Cheah, P. Fornasiero, F. Kemausuor, S. Zinoviev and S. Miertus, *ChemSusChem* **2009**, *2*, 278-300.
- [4] H. Li, Z. Fang, J. Luo and S. Yang, *Appl. Catal. B: Environ.* **2017**, *200*, 182-191.
- [5] G. Morales, A. Osatiashtiani, B. Hernandez, J. Iglesias, J. A. Melero, M. Paniagua, D. R. Brown, M. Granollers, A. F. Lee and K. Wilson, *Chem. Commun.* **2014**, *50*, 11742-11745.
- [6] B. C. Windom, T. M. Lovestead, M. Mascal, E. B. Nikitin and T. J. Bruno, *Energ. Fuel.* **2011**, *25*, 1878-1890.
- [7] E. Ahmad, M. I. Alam, K. K. Pant and M. A. Haider, *Green Chem.* **2016**, *18*, 4804-4823.
- [8] S. Saravanamurugan and A. Riisager, *ChemCatChem* **2013**, *5*, 1754-1757.
- [9] L. Jiang, L. Zhou, J. Chao, H. Zhao, T. Lu, Y. Su, X. Yang and J. Xu, *Appl. Catal. B: Environ.* **2018**, *220*, 589-596.
- [10] S. Saravanamurugan and A. Riisager, *Catal. Commun.* **2012**, *17*, 71-75.
- [11] C. H. Kuo, A. S. Poyraz, L. Jin, Y. Meng, L. Pahalagedara, S. Y. Chen, D. A. Kriz, C. Guild, A. Guduz and S. L. Suib, *Green Chem.* **2014**, *16*, 785-791.
- [12] R. Liu, J. Chen, X. Huang, L. Chen, L. Ma and X. Li, *Green Chem.* **2013**, *15*, 2895-2903.
- [13] A. Takagaki, M. Ohara, S. Nishimura and K. Ebitani, *Chem. Commun.* **2009**, *0*, 6276-6278.
- [14] L. Zhou, H. Zhao, L. Cui, Y. Bai, J. Bian, T. Lu, Y. Su and X. Yang, *Catal. Commun.* **2015**, *71*, 74-78.
- [15] I. Delidovich and R. Palkovits, *ChemSusChem* **2016**, *9*, 547-561.
- [16] H. Nguyen, V. Nikolakis and D. G. Vlachos, *ACS Catal.* **2016**, *6*, 1497-1504.
- [17] J. M. R. Gallo, D. M. Alonso, M. A. Mellmer and J. A. Dumesic, *Green Chem.* **2013**, *15*, 85-90.
- [18] F. Chen, H. Ma and B. Wang, *J. Hazard. Mater.*, **2009**, *162*, 668-673.
- [19] J. Gardy, A. Hassanpour, X. Lai, M. H. Ahmed and M. Rehan, *Appl. Catal. B: Environ.* **2017**, *207*, 297-310.
- [20] Z. Li, R. Wnetrzak, W. Kwapinski and J. J. Leahy, *ACS appl. Mater. Inter.* **2012**, *4*, 4499-4505.
- [21] E. M. Domingues, N. Bion, F. M. Figueiredo and P. Ferreira, *Micropor. Mesopor. Mat.* **2016**, *226*, 386-395.
- [22] J. Valmaña-Traverso, S. Morante-Zarcelo, D. Pérez-Quintanilla, M. Á. García, I. Sierra and M. L. Marina, *J.Chromatogr. A* **2018**, *1566*, 135-145.

- [23] M. G. Goesten, Á. Szécsényi, M. F. de Lange, A. V. Bavykina, K. B. S. S. Gupta, F. Kapteijn and J. Gascon, *ChemCatChem* **2016**, *8*, 961-967.
- [24] S. Suganuma, K. Nakajima, M. Kitano, D. Yamaguchi, H. Kato and S. Hayashi, *J. Am. Chem. Soc.* **2008**, *130*, 12787-12793.
- [25] F. Su, Q. Wu, D. Song, X. Zhang, M. Wang and Y. Guo, *J. Mater. Chem. A* **2013**, *1*, 13209-13221.
- [26] X. Zhang, Y. Zhao and Q. Yang, *J. Catal.* **2014**, *320*, 180-188.
- [27] D. Song, S. An, Y. Sun and Y. Guo, *J. Catal.* **2016**, *333*, 184-199;
- [28] J. Liu, S. Y. Bai, H. Zhong, C. Li and Q. H. Yang, *J. Phys. Chem. C* **2010**, *114*, 953-961.
- [29] Z. Teng, X. Su, Y. Zheng, J. Zhang, Y. Liu, S. Wang, J. Wu, G. Chen, J. Wang, D. Zhao and G. Lu, *J. Am. Chem. Soc.* **2015**, *137*, 7935-7944.
- [30] A. M. Alsalme, P. V. Wiper, Y. Z. Khimiyak, E. F. Kozhevnikova and I. V. Kozhevnikov, *J. Catal.* **2010**, *276*, 181-189.
- [31] M. G. Kulkarni, R. Gopinath, L. C. Meher and A. K. Dalai, *Green Chem.* **2006**, *8*, 1056-1062.
- [32] W. Li, F. Ma, F. Su, L. Ma, S. Zhang and Y. Guo, *ChemSusChem* **2011**, *4*, 744-756.
- [33] K. Arata, *Green Chem.* **2009**, *11*, 1719-1728.
- [34] V. Adeeva, J. W. Dehaan, J. Janchen, G. D. Lei, V. Schunemann, L. J. M. Vandeven, W. M. H. Sachtler and R. A. Vansanten, *J. Catal.* **1995**, *151*, 364-372.
- [35] P. Lanzafame, K. Barbera, S. Perathoner, G. Centi, A. Aloise, M. Migliori, A. Macario, J. B. Nagy and G. Giordano, *J. Catal.* **2015**, *330*, 558-568.
- [36] D. Song, Y. Sun, Q. Zhang, P. Zhang, Y. Guo and J. Leng, *Appl. Catal. A: Gen.* **2017**, *546*, 36-46.
- [37] L. Peng, L. Lin, J. Zhang, J. Shi and S. Liu, *Appl. Catal. A: Gen.* **2011**, *397*, 259-265.
- [38] G. D. Yadav, N. P. Ajgaonkar and A. Varma, *J. Catal.*, **2012**, *292*, 99-110.
- [39] Z. Cheng, J.L. Everhart, G. Tsilomelekis, V. Nikolakis, B. Saha, and D. G. Vlachos, *Green Chem.* **2018**, *20*, 997-1006.
- [40] F. Liu, K. Huang, A. Zheng, F.-S. Xiao and S. Dai, *ACS Catal.* **2017**, *8*, 372-391.
- [41] J. A. Melero, G. D. Stucky, R. van Grieken and G. Morales, *J. Mater. Chem.* **2002**, *12*, 1664-1670.

Entry for the Table of Contents

FULL PAPER

$\text{SO}_4^{2-}/\text{ZrO}_2\text{-PMO-SO}_3\text{H}$ catalysts with super strong Brønsted acidity and moderate Lewis acidity exhibit high yield of ethyl levulinate from glucose conversion.



Daiyu Song,^[a] Qingqing Zhang,^[a]
Yingnan Sun,^[a] Panpan Zhang,^[a] Yi-
Hang Guo,^{* [a]} and Jiang-Lei Hu^{*[b]}

Page No. – Page No.

Design of ordered mesoporous
sulfonic acid functionalized
 ZrO_2 /organosilica bifunctional
catalysts for direct catalytic
conversion of glucose to ethyl
levulinate